Title

A Rabbit Model to Study Antibiotic Penetration at the Site of Infection for Nontuberculous Mycobacterial Lung Disease: Macrolide Case Study

Journal

Antimicrobial Agents and Chemotherapy, 66(3)

ISSN

0066-4804

Authors

Kaya, Firat
Ernest, Jacqueline P
LoMauro, Katherine
et al.

Publication Date

2022-03-15

DOI

10.1128/aac.02212-21

Peer reviewed

AMERICAN SOCIETY FOR MICROBIOLOGY | Antimicrobial Agents and Chemotherapy®

PHARMACOLOGY

A Rabbit Model to Study Antibiotic Penetration at the Site of Infection for Nontuberculous Mycobacterial Lung Disease: Macrolide Case Study

Firat Kaya,[a] Jacqueline P. Ernest,[b] Katherine LoMauro,[a] Martin Gengenbacher,[a,c] Abdeldjalil Madani,[a] Wassihun Wedajo Aragaw,[a] Matthew D. Zimmerman,[a] Jansy P. Sarathy,[a] Nadine Alvarez,[a] Isaac Daudelin,[d] Han Wang,[a] Faye Lanni,[a] Danielle M. Weiner,[e] Laura E. Via,[e,f] Clifton E. Barry III,[e,f] Kenneth N. Olivier,[g] Thomas Dick,[a,c,h] Brendan K. Podell,[i] Radojka M. Savic,[b] Véronique Dartois[a,c]

[a]Center for Discovery and Innovation, Hackensack Meridian Health, Nutley, New Jersey, USA
[b]Department of Bioengineering and Therapeutic Sciences, University of California, San Francisco, San Francisco, California, USA
[c]Hackensack Meridian School of Medicine, Department of Medical Sciences, Nutley, New Jersey, USA
[d]New Jersey Medical School, Rutgers, The State University of New Jersey, Newark, New Jersey, USA
[e]Tuberculosis Research Section, Laboratory of Clinical Immunology and Microbiology, NIAID, NIH, Bethesda, Maryland, USA
[f]Institute of Infectious Disease and Molecular Medicine, Faculty of Health Sciences, Cape Town, South Africa
[g]Laboratory of Chronic Airway Infection, Pulmonary Branch, National Hearth Lung Blood Institute, NIH, Bethesda, Maryland, USA
[h]Department of Microbiology and Immunology, Georgetown University, Washington, DC, USA
[i]Mycobacteria Research Laboratories, Department of Microbiology, Immunology and Pathology, College of Veterinary Medicine and Biomedical Sciences, Colorado State University, Fort Collins, Colorado, USA

Firat Kaya and Jacqueline P. Ernest contributed equally to this article. Author order was determined in order of seniority.

ABSTRACT Nontuberculous mycobacterial pulmonary disease (NTM-PD) is a potentially fatal infectious disease requiring long treatment duration with multiple antibiotics and against which there is no reliable cure. Among the factors that have hampered the development of adequate drug regimens is the lack of an animal model that reproduces the NTM lung pathology required for studying antibiotic penetration and efficacy. Given the documented similarities between tuberculosis and NTM immunopathology in patients, we first determined that the rabbit model of active tuberculosis reproduces key features of human NTM-PD and provides an acceptable surrogate model to study lesion penetration. We focused on clarithromycin, a macrolide and pillar of NTM-PD treatment, and explored the underlying causes of the disconnect between its favorable potency and pharmacokinetics and inconsistent clinical outcome. To quantify pharmacokinetic-pharmacodynamic target attainment at the site of disease, we developed a translational model describing clarithromycin distribution from plasma to lung lesions, including the spatial quantitation of clarithromycin and azithromycin in mycobacterial lesions of two patients on long-term macrolide therapy. Through clinical simulations, we visualized the coverage of clarithromycin in plasma and four disease compartments, revealing heterogeneous bacteriostatic and bactericidal target attainment depending on the compartment and the corresponding potency against nontuberculous mycobacteria in clinically relevant assays. Overall, clarithromycin's favorable tissue penetration and lack of bactericidal activity indicated that its clinical activity is limited by pharmacodynamic, rather than pharmacokinetic, factors. Our results pave the way toward the simulation of lesion pharmacokinetic-pharmacodynamic coverage by multidrug combinations to enable the prioritization of promising regimens for clinical trials.

KEYWORDS clarithromycin, animal model, tissue penetration, nontuberculous mycobacteria, lung pathology, macrolides

Address correspondence to Véronique Dartois, veronique.dartois@hmh-cdi.org.

The authors declare no conflict of interest.

Received 23 November 2021
Returned for modification 20 December 2021
Accepted 17 January 2022
Accepted manuscript posted online 31 January 2022
Published 15 March 2022

Nontuberculous mycobacteria (NTM) are environmental mycobacteria related to *Mycobacterium tuberculosis* and can cause progressive, fatal pulmonary disease (NTM-PD) (1). NTM-PD occurs in patients with immunodeficiencies, structural lung damage, or both. The immunopathology that develops in NTM-PD patients is partially driven by these preexisting conditions (2). In immunocompromised patients, where the cause of immunosuppression is either genetic or induced by drug treatment or human immunodeficiency virus (HIV) infection, disease manifestations include extrathoracic disease, poorly formed granulomatous structures, diffuse consolidation, and miliary disease, all consistent with systemic immune dysfunction and reminiscent of tuberculosis (TB)-HIV (2–4). In immunocompetent patients with bronchiectatic conditions—chronic obstructive pulmonary disease (COPD) and cystic fibrosis (CF) being the most common—nodular or cavitary pathology, necrosis, and worsening bronchiectasis are frequently seen (5–7). These presentations bear key similarities with TB in immunocompetent subjects (8), where the most common microscopic finding is necrotizing granulomas and cavities, characterized by a central zone of necrosis surrounded by a variably thick rim of macrophages, neutrophils, lymphocytes, and fibroblasts. As seen in TB, necrotic lesions have also been found in the lymph nodes of NTM-PD patients, particularly in those with HIV (9). Cavities in NTM-PD are similar to pulmonary TB cavities with subtle differences such as a thinner fibrotic wall as detected by computed tomography (10–12) and enhanced associated pleural thickening (13). Although cavitary disease is overall less frequent in NTM-PD than TB patients (14), the presence of large cavities is associated with disease progression leading to respiratory failure and high mortality rate (15). There is consensus in the clinical field that differentiating NTM-PD from pulmonary TB solely based on radiologic findings is not recommended due to considerable overlap in the clinical and radiographic features of pulmonary TB and NTM-PD (16, 17). Histologic feature similarities between TB and NTM disease, and their relative frequencies, have been extensively reviewed by Jain et al. (18).

Surgical resections, which have been practiced since the 1960s until today, when disease is localized, show gross and histopathologic findings identical to the manifestation usually associated with typical *M. tuberculosis* infection (13, 19). Histology and acid-fast stains of resected cavities have revealed bacterial aggregates or heaps along the inner wall of cavities (8, 20, 21). More recently, scanning electron microscopy of the inner wall of a resected cavity demonstrated bacilli embedded within a matrix (20). High bacterial burden ($>10^7$ CFU) was enumerated in a 0.5-g sample from the lung cavity, a significant fraction of which were in biofilm-like structures (6).

Clarithromycin and azithromycin, broad-spectrum macrolides, are the pillar of NTM treatment. Most NTM-PD patients are treated with a macrolide-containing multidrug regimen until they remain sputum negative for 12 consecutive months (22). Despite such intensive therapy and the adequate potency of clarithromycin against susceptible NTM strains, treatment failures and relapse rates are high, particularly for *M. abscessus* disease (23, 24). Understanding the underlying causes of such disconnects is important if we are to optimize existing drug regimens and develop more effective ones.

Macrolide antibiotics accumulate in phagocytic cells (25) and preferentially distribute in tissues where populations of these cells reside (26). A beneficial consequence of high uptake in host cells is increased activity against intracellular pathogens (27). In addition, phagocytes may serve as a vehicle that transports macrolides to the site of infection (tissue-directed pharmacokinetics) (28, 29). Indeed, tissue and intracellular concentrations may be more useful for assessing the antibacterial activity of macrolides than plasma concentrations (30). Accordingly, tissue pharmacokinetic-pharmacodynamic (PK-PD) concepts have been proposed for macrolides (31), and therapeutic drug monitoring in plasma is not recommended (32). While accumulation in phagocytes positively contributes to bacterial eradication, the heterogeneous sites of NTM-PD disease in patient populations with diverse manifestations (18) may provide the ground for subtherapeutic clarithromycin coverage of poorly vascularized compartments where the pathogen resides, as seen for some TB drugs (33). *In vitro*, clarithromycin is used as the representative macrolide in drug susceptibility assays owing to better solubility at high concentrations than azithromycin (34). Interestingly, clarithromycin treatment

may lead to higher *erm*41-mediated induction of macrolide resistance in *M. abscessus* than azithromycin (35), though this remains a matter of debate (36, 37). Clarithromycin is mostly bacteriostatic against replicating NTM cultures and intracellular bacteria in macrophages (38), although longer incubation times have delivered bactericidal activity at 16 mg/L and above against replicating *M. abscessus* in cation-adjusted Mueller-Hinton broth (39). It lacks bactericidal activity against NTM in biofilms (38) and slow-replicating or nonreplicating persisters (40). Thus, there is a disconnect between clarithromycin growth inhibitory activity (MIC) measured in clinical practice and activity against mycobacterial subpopulations at the sites of disease. Collectively, pharmacokinetic and pharmacodynamic observations suggest heterogeneous coverage of the sites of disease and bacterial populations in macrolide-susceptible NTM-PD.

Despite significant efforts dedicated to the development of animal models of NTM disease (41–43), we still lack an immunocompetent model that presents organized cellular and necrotic lesions and reasonably reproduces the human lung pathology required for studying antibiotic penetration (44). Here, we first determine that the rabbit model of active TB disease provides an acceptable surrogate for studying pharmacokinetics at the site of NTM-PD. Taking advantage of TB and NTM-PD pathology similarities, we quantify the distribution of clarithromycin in mycobacterial lesion compartments following multiple human-equivalent oral doses to rabbits with active TB. We compare these results to a limited data set of clarithromycin and azithromycin in mycobacterial lung lesions from patients on long-term macrolide therapy. To assess the potential efficacy of clarithromycin at the sites of disease in healthy and immunocompromised subjects, we relate these concentrations to those required to inhibit growth of or kill nontuberculous mycobacteria in standard culture media, biofilms, and macrophages. Future studies of similar design with other NTM drugs could help rationalize differential clinical responses of patients with a spectrum of disease presentation and immunopathology.

RESULTS

The rabbit model of active TB reproduces major histopathology features of clinical NTM-PD. Given the lack of NTM animal models with pathological features comparable to human clinical NTM disease, we assessed the histopathological similarities between the rabbit model of active TB, clinical NTM disease, and clinical TB disease in human patients (Fig. 1) to evaluate the suitability of the rabbit TB model for lesion penetration of NTM drugs. Key pulmonary sites of infection where drugs show differential partitioning are the cellular and necrotic regions of granulomas and cavities.

Similar to the rabbit model of TB, human clinical NTM infection develops structured granulomas, including central caseous necrosis with a paucicellular inner caseum and greater neutrophil composition at the outer caseum margin. The central necrosis is surrounded by a layer of lipid-loaded macrophages and an outer cellular cuff with greater lymphocyte abundance, fibrosis, and pulmonary epithelium (Fig. 1A and B). These features are all similarly represented in both the rabbit model of TB (Fig. 1C and D) and human clinical TB (Fig. 1E and F). Collectively, the pulmonary tissue from human clinical NTM infection demonstrated a heterogeneous profile of lesions over chronic disease and lengthy antimicrobial treatment (Fig. S1 in the supplemental material). Aside from an abundance of granuloma lesions similar to the rabbit TB model, these features also included fibrosis in perilesional lung, pleural, and alveolar interstitium and the presence of secondary lymphoid follicle-like structures. Several heterogeneous and/or occasional features of clinical NTM-PD, such as coalescing nonnecrotic granulomas, cavitary necrotic lesions with abundant caseum, and bronchioles filled with necrotic caseum containing neutrophils, indicative of bronchogenic spread as seen in human TB (45, 46), were also observed in rabbits with active TB (Fig. S2). Comparable immunohistopathology of NTM and TB lung disease has been reported by others (12, 18). Thus, the rabbit model of active TB reproduces key pathological features of clinical NTM-PD and is a useful tool for evaluating drug penetration at key pulmonary sites of mycobacterial infection.

***In vitro* prediction of macrolide partitioning in cellular and necrotic lesion areas.** Previous work by our group indicated that drug penetration in cellular granulomas and partitioning between the cellular rim and necrotic core of lung lesions is a function

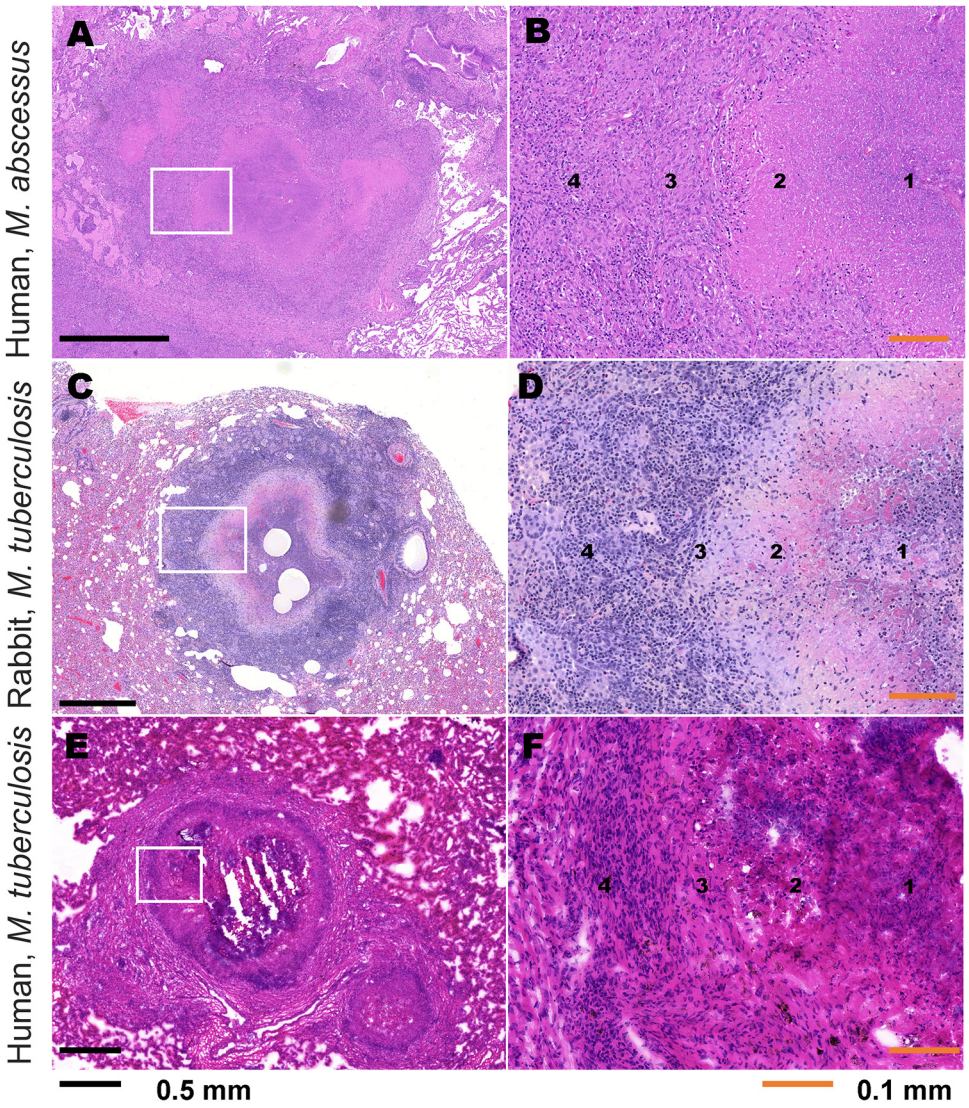

FIG 1 Comparative histopathology of human clinical NTM infection, *M. tuberculosis* infection in the rabbit model, and human clinical *M. tuberculosis* infection. (A) H&E-stained image of representative NTM granuloma lesion in the lung of human patient with clinical NTM infection caused by *M. abscessus*. (B) Higher magnification of inset region in panel A demonstrating microenvironmental locations, labeled 1 to 4. (C) H&E-stained image of representative granuloma lesion in the lung of an *M. tuberculosis*-infected rabbit. (D) Higher magnification of inset region in panel C demonstrating microenvironmental locations, labeled 1 to 4. (E) H&E-stained image of representative TB granuloma lesion in the lung of a human patient with clinical *M. tuberculosis* infection. (F) Higher magnification of inset region in panel E demonstrating microenvironmental locations, labeled 1 to 4. 1, inner caseum; 2, outer caseum and neutrophil rim; 3, macrophage layer; 4, lymphocyte-rich cellular and collagen rim.

of (i) uptake into immune cells *in vitro* (47), and (ii) binding to caseum macromolecules (48, 49). The fate of drug molecules at the outer edge of caseum is a balance between uptake into the bordering macrophages, binding to macromolecules, and effective diffusion into nonvascularized caseum. In necrotizing granulomas, intracellular *M. tuberculosis* is found in macrophages (12, 18, 50). In response to infection and low oxygen tension caused by decreased vascular efficiency (51, 52), macrophages accumulate lipid bodies and become foamy. These foamy infected macrophages necrotize and release their bacterial and cellular contents into the central caseum.

To predict the distribution of clarithromycin and azithromycin in cellular and necrotic lesion compartments, we measured drug binding in *ex vivo* caseum and uptake into primary human macrophages—foamy and nonfoamy—derived from blood monocytes. The average unbound fraction in caseum (f_u-caseum) was 3% to 5%, thus moderate to low for both drugs

TABLE 1 *In vitro* lesion pharmacokinetic profiling of macrolides clarithromycin and azithromycin

	Uptake in primary human macrophages (intracellular-to-extracellular concentration ratio) for:[a]					
	Clarithromycin[c]			Azithromycin[c]		
Macrophage type	Donor 1[b]	Donor 2	Donor 3	Donor 1	Donor 2	Donor 3
Standard differentiated macrophages	95.0 ± 13.3	38.6 ± 16.9	106.2 ± 7.2	75.6 ± 3.0	46.8 ± 14.9	114.6 ± 14.3
Foamy macrophages	98.5 ± 2.8	32.2 ± 7.0	89.8 ± 19.5	86.5 ± 10.0	37.7 ± 8.1	95.8 ± 12.6

[a]Data represent mean ± SD. $n = 3$ replicates.
[b]Human monocytes were isolated from fresh packed leucocytes of three independent anonymous donors (different from the two subjects who underwent lung resection and contributed the tissues analyzed for drug content).
[c]Free caseum fraction (mean ± SD) for clarithromycin, 3.9 ± 0.1%, and for azithromycin, 5.4 ± 0.4%.

(Table 1). Intracellular uptake was measured in primary human macrophages, including macrophages where the foamy phenotype was induced by infection with irradiated *M. tuberculosis* (47). We observed high intracellular accumulation in blood-derived human macrophages and similar accumulation in foamy and nonfoamy macrophages (Table 1), indicative of favorable penetration and higher concentrations in cellular lesions than in plasma. Together with the relatively low f_u-caseum, high intracellular uptake predicted limited or slow passive diffusion through nonvascularized caseum. To confirm these predictions, we measured clarithromycin concentrations at the site of mycobacterial disease in the rabbit model of active TB, which presents with cellular granulomas, necrotic lesions, and cavities.

Clarithromycin exhibits differential penetration into mycobacterial lung lesions. Clarithromycin was selected as a representative macrolide used to treat NTM-PD (53, 54). To study and model the penetration of clarithromycin in lung lesions, we first identified a rabbit dose that achieves exposure comparable to that of NTM patients receiving 500 mg daily (55–60). The concentration-time profile was established in naive (uninfected) rabbits following single oral doses of 100 mg/kg and 300 mg/kg and three daily doses of 300 mg/kg (Fig. S3A and Table 2). The area under the concentration-time curve (AUC)/MIC ratio is considered the primary PK-PD parameter driving the antibacterial effect of clarithromycin and azithromycin (61–63). To reproduce the AUC achieved in humans following repeated oral daily doses of 500 mg, we selected 200 mg/kg for subsequent tissue and lesion penetration studies in rabbits (Fig. S3B and Table 2).

To build a translational model of clarithromycin penetration at the site of mycobacterial lung disease, we measured drug concentrations in serial blood samples, uninvolved lung tissue, and lesion homogenates in groups of 3 infected rabbits following three daily 200-mg/kg doses. Tissue samples were collected 6 h (end of the distribution phase) and 24 h (trough) after the third dose. The total number of observations and the concentrations of clarithromycin in plasma, uninvolved lung, and cellular and necrotic lesions are shown in Fig. 2A and Data Set S1. In line with the high intracellular uptake in macrophages, total clarithromycin concentrations were 30- to 40-fold higher in uninvolved lung (devoid of macroscopic lesions but infiltrated with various immune cell types) than in plasma and over 100-fold higher in cellular lesions than in plasma (Fig. 2A). In caseum isolated from a large cavity at 24 h, clarithromycin was present at a higher concentration than in plasma but lower than average concentrations in cellular lesions. To confirm this initial observation and better describe the partitioning of clarithromycin at the interface between cellular rims and caseous (necrotic) foci, we reserved

TABLE 2 Clarithromycin plasma pharmacokinetic parameters in rabbits compared to humans at the clinical dose[a]

Dose (no. of doses)	C_{max} (ng/mL)	T_{max} (h)	AUC_{0-24} (ng·h/mL)
100 mg/kg (single dose)	427 ± 286	3 ± 1	3,762 ± 3,365
300 mg/kg (single dose)	2,828 ± 1,001	4 ± 1.5	28,409 ± 12,317
300 mg/kg (3 daily doses)	4,158 ± 916	1.4 ± 0.8	28,543 ± 8,790
200 mg/kg (3 daily doses in infected rabbits)	1,938 ± 1,073	1.50 ± 0.55	11,709 ± 4,922
Target human PK parameters (500 mg at steady state) (56–58, 60)	2,500 – 3,000	2-3 h	18,000 – 20,000

[a]Data represent mean ± SD. C_{max}, peak plasma concentration; T_{max}, time of peak plasma concentration; AUC_{0-24}, area under the concentration-time curve from 0 to 24 h.

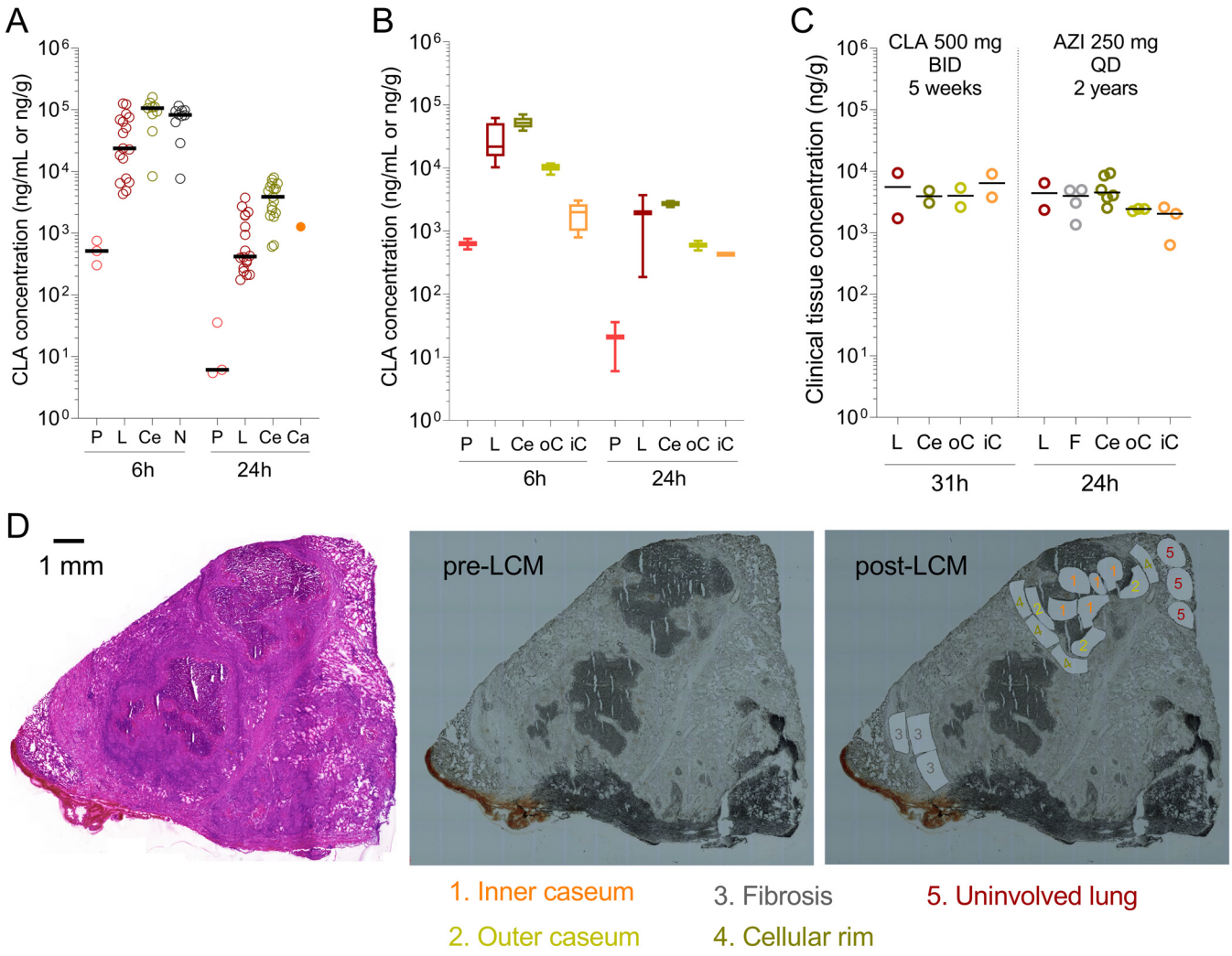

FIG 2 Distribution of clarithromycin from plasma into major pulmonary lesion compartments. (A) Clarithromycin concentrations in rabbit plasma, lung, and whole-lesion homogenates after 3 daily doses. P, plasma; L, uninvolved lung (devoid of macroscopically visible lesions); Ce, fully cellular lesion; N, partially necrotic lesion; Ca, cavity caseum. Each data point represents one individual plasma or tissue sample; $n = 3$ rabbits per time point. (B) Spatial quantitation of clarithromycin in large necrotic rabbit lesions by laser-capture microdissection. P, plasma; L, uninvolved lung; Ce, cellular rim; oC, outer edge of caseum adjacent to the cellular rim; iC, inner core of caseum. Lesions were collected from a subset of the animals shown in panel A. (C) Spatial quantitation of clarithromycin and azithromycin in large lesions collected from the resected lung of a TB patient (left) and an *M. abscessus* disease patient (right), respectively. L, uninvolved lung; F, fibrotic cuff; Ce, cellular rim; oC, outer edge of caseum; iC, inner core of caseum. (D) Typical example of histology staining and laser capture microdissection (LCM) of thin human lesions sections. Two large necrotic lesions were collected from the resected lung tissue of human subject G-101 receiving CLA 1,000 mg QD. The adjacent tissue section was used for hematoxylin and eosin (H&E) staining (left) to guide LCM sample collection (right). 1, inner caseum; 2, outer caseum; 3, fibrosis; 4, cellular rim; 5, uninvolved lung. Color coding of tissue compartments is identical to panels A to C. Laser-dissected pieces belonging to the same tissue compartment were pooled for quantitation by LC-MS/MS.

large necrotic lesions from the same animals for laser-capture microdissection (LCM) in thin tissue sections (64). Concentrations in uninvolved lung and cellular rims matched the corresponding concentrations measured in lung tissue and cellular lesion homogenates (Fig. 2B). We found the highest clarithromycin concentrations in cellular rims, gradually decreasing as one moves inward into the caseum periphery and deep caseum, in line with the limited f_u-caseum measured *in vitro*. The trend of concentration gradients was similar at 6 h and 24 h. However, clarithromycin appeared to gradually diffuse into deep caseum between 6 and 24 h, reducing the caseum/cellular concentration ratio (Fig. 2B). To confirm this observation, we applied LCM to clinical lung samples resected from (i) a TB patient who had received clarithromycin 1,000 mg once daily (QD) for 5 weeks as salvage therapy, and (ii) an *M. abscessus* patient who had been on azithromycin 250 mg QD for approximately 2 years. Resections took place 31 h and 24 h after the last macrolide dose, respectively. We found that drug concentrations measured at trough in lung and cellular rims were similar in these

TABLE 3 Plasma-to-tissue model parameters[a]

Compartment	Parameter	Value (RSE [%])
Plasma	V_{max} (L/h)	88.72 (18.5)
	K_m (mg/L)	0.3862 (36.6)
	V	207.2 (26.4)
	K_w	0.1776 (145.9)
	λ	0.6028 (58.5)
	Q	157.5 (34.9)
	V_2	393.4 (13.6)
	IIV F1	0.3311 (14.5)
	Additive error (mg/L)	0.0071 (48.2)
	Proportional error (%)	45.66 (8.0)
Lung	Partition coefficient	67.9 (35.6)
	Plasma-to-tissue rate constant (1/h)	10 (FIX)
	Proportional error (%)	108 (12)
Cellular lesion	Partition coefficient	102 (16.2)
	Plasma-to-tissue rate constant (1/h)	0.283 (13.4)
	Proportional error (%)	70.5 (16.2)
Outer caseum	Partition coefficient	13.1 (20.0)
	Plasma-to-tissue rate constant (1/h)	0.265 (14.2)
	Proportional error (%)	39.6 (21.8)
Inner caseum	Partition coefficient	2.86 (9)
	Plasma-to-tissue rate constant (1/h)	0.174 (5.3)
	Proportional error (%)	32.6 (24)

[a]RSE, relative standard error; V_{max}, maximum rate of clearance; K_m, Michaelis-Menten constant; V, central volume of distribution; K_w, absorption rate constant; λ, shape parameter; Q, intercompartmental clearance; V_2, peripheral volume of distribution; IIV, interindividual variability; F1, apparent bioavailability. FIX, parameter was fixed.

two subjects and rabbits after three daily 200-mg/kg doses (Fig. 2C). Interestingly, the decreasing drug concentration from the cellular rim into deep caseum was much shallower in these patients, who were in advanced steady state, than in rabbits after 3 doses. Specifically, clarithromycin partitioned evenly across all lesion compartments, including deep caseum, while azithromycin was only 2- to 3-fold lower in caseum than in cellular regions (Fig. 2C). This suggests that, as suspected, macrolides equilibrate slowly into nonvascularized caseum and that steady state appears to be achieved in caseum after QD dosing for 5 weeks but not after three daily doses in rabbits.

To quantitatively describe the differential penetration of clarithromycin in mycobacterial lung lesions, we developed a multicompartment nonlinear mixed-effects PK model. The final plasma model was a two-compartment model with Weibull absorption, which is a flexible model function that better describes slow onset absorption with gradual acceleration (65), and Michaelis-Menten elimination. Infection status and weight were not identified as covariates of drug exposure. Replacing first-order absorption with Weibull absorption significantly improved model fit, with a delta objective function value (dOFV) of −52.743. Clarithromycin accumulated in regions of high cellularity (uninvolved lung and cellular lesions) with total AUC of tissue (AUC_{tissue}) approximately 2 orders of magnitude higher than total AUC_{plasma}. Cellular lesions had the largest partition coefficient, which was 102. Necrotic areas, including the outer caseum (the region adjacent to the cellular rim of the necrotic core) and inner caseum (the center of large necrotic lesions) of closed lesions and cavities, also had high clarithromycin concentration relative to plasma, with partition coefficients of 13.1 and 2.9, respectively (Table 3). Clarithromycin distribution to lesions, but not to uninvolved lung, was slow, with concentrations peaking 2 to 4 h after the peak concentration of plasma (T_{max}). Visual predictive checks indicated that the final model fit the data well (Fig. 3).

Clarithromycin exhibits differential pharmacokinetic-pharmacodynamic coverage of major lesion compartments. Clarithromycin inhibits growth of most replicating NTM strains below 1 μg/mL but has no bactericidal activity up to 20 to 256 μg/mL, depending on the strains and assay conditions (38, 66). To confirm these observations and place lesion concentrations of clarithromycin into pharmacodynamic context at the site of disease, we measured, side by side, (i) the MIC and minimal bactericidal concentration (MBC) against

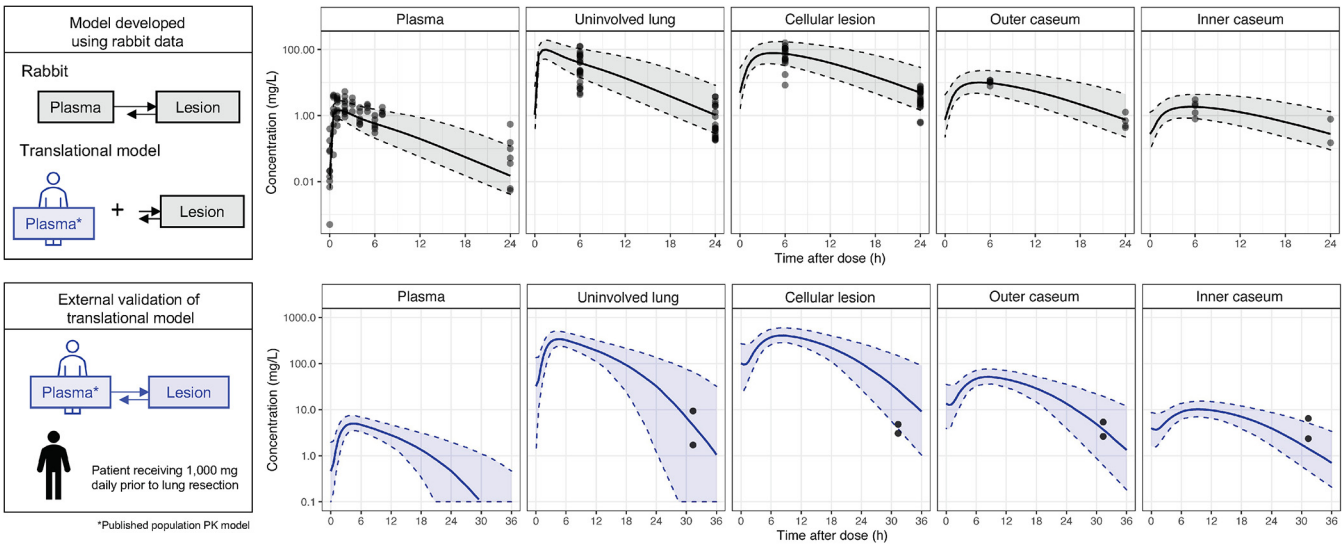

FIG 3 Visual predictive check of clarithromycin rabbit plasma-to-tissue multicompartment model. The translational model was built by integrating a population PK model with lesion parameters estimated in rabbits. (Top) Observed clarithromycin concentrations (individual dots) in rabbits, with 500 simulations represented as median (solid line) and 5th and 95th percentiles (gray shaded area, dashed lines). To externally validate the model, we simulated clarithromycin penetration in 4 lesion compartments following a 1,000-mg daily dose to steady state (n = 500) and compared with pulmonary drug levels of one patient who received 1,000 mg once daily for 5 weeks prior to lung resection. (Bottom) Patient clarithromycin observations from two biopsy specimens (individual dots) with 500 simulations represented as median (solid line) and 5th and 95th percentiles (blue shaded area, dashed lines).

representative clinical isolates of *M. abscessus* and *M. avium* in standard growth media (Table 4; Fig. S4A to D), and (ii) the concentrations required for growth inhibition and killing of intracellular *M. abscessus* and *M. avium* in macrophages (Fig. S5). Since *M. abscessus* and *M. avium* have been found in aggregates described as heaps (21), large clumps (67), or biofilms (20) in the lungs of NTM-PD patients, we retrieved from the literature the concentrations required to inhibit biofilm formation and kill *M. abscessus* and *M. avium* in established biofilms and against nonreplicating NTM bacteria (38, 40) (Table 4). We also confirmed that clarithromycin lacks bactericidal activity against planktonic *M. abscessus* and *M. avium* up to 25 μM (~20 μg/mL) and exhibits limited bactericidal activity (approximately 5-fold kill) against intracellular *M. avium* only up to 25 μM, without reaching the MBC_{90} (Fig. S4 and S5). These potency values were used to simulate lesion PK-PD coverage in human lung lesions.

To predict concentrations within patient lungs and lesions, a published clinical model (55) was integrated with the rabbit plasma-to-lesion model, and a clinical dose of 500 mg administered twice daily was simulated. To assess the predictive ability of the translational model, we simulated pulmonary tissue distribution following a 1,000-mg dose, reproducing a patient

TABLE 4 *In vitro* potency of clarithromycin in representative growth inhibitory and bactericidal assays

	Data (reference or source) for:[g]	
Parameter	***M. abscessus***	***M. avium***
Susceptibility breakpoints or ECOFF[a]	<4, susceptible; 4–8, intermediate; >8, resistant (103)	<2, susceptible (104)
MIC_{90}[b]	0.2–1.2	0.15–1.2
MBC_{90}	>20 (this work)	20 (this work)
Intracellular IC_{90}	0.1[c]	0.2,[c] 0.05[d] (105)
Intracellular MBC_{90}[e]	>25 μg/mL	> 0 μg/mL
Biofilm MIC_{90}	2.2 (40)	2 μg/mL (90)
Biofilm MBC_{90}	>75 μg/mL (40), 256 μg/mL (38)	>20 μg/mL (106, 107)
Nonreplicating nutrient starvation MBC_{90}	256 μg/mL (39)	ND[f]

[a]Against multiple subspecies and isolates.
[b]In this work, 90% growth inhibition against a panel of susceptible reference strains.
[c]In this work, 90% growth inhibition of *M. abscessus* subsp. *abscessus* ATCC 19977 and *M. avium* subsp. *hominisuis* 11 in THP-1 macrophages.
[d]*M. avium* was grown in A549 lung epithelial cells.
[e]In this work, bactericidal activity (90% killing) against *M. abscessus* ATCC 19977 and *M. avium* 11 in THP-1 macrophages.
[f]ND, not determined.
[g]All data are given as μg/mL.

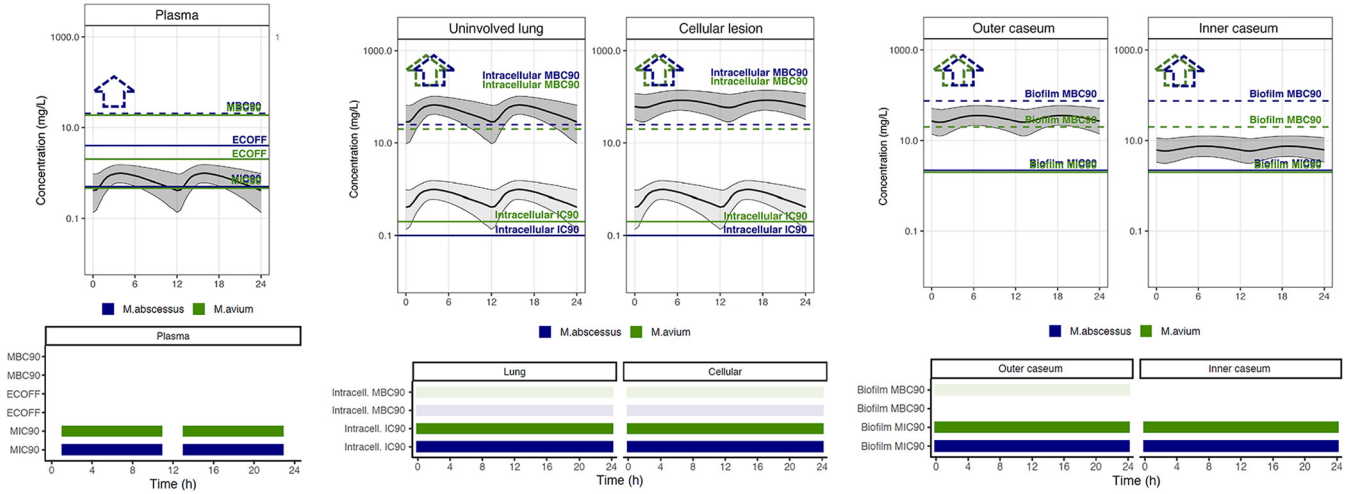

FIG 4 Clinical simulations of clarithromycin PK-PD coverage in plasma and four lung compartments. Steady-state pharmacokinetic profiles are shown for one 24-h period following administration of 500 mg clarithromycin twice daily. One thousand simulations were performed with the translational model and are represented as the median (solid black line) and 5th and 95th percentiles (thin black lines and gray shaded area). Plasma concentrations were corrected for protein binding (f_u, 30%). In uninvolved lung and cellular lesions, the dark gray shaded profile was simulated using total clarithromycin tissue concentrations, and the light gray shaded profile assumes passive diffusion of free drug from plasma to interstitial tissue. *In vitro* targets are represented as horizontal lines and colored by mycobacterial species (*M. abscessus*, blue; *M. avium*, green). Dotted lines accompanied by dotted line arrows indicate PD targets greater than the highest concentration tested *in vitro*. In PK-PD coverage plots shown under each concentration-time profile, colored boxes indicate periods during which clarithromycin concentrations are above the corresponding *in vitro* PD target indicated on the left of each row (*M. abscessus*, blue; *M. avium*, green). The MIC_{90} was set at 0.6 μg/mL or the average of the MIC_{90}s measured against a panel of susceptible reference strains as part of this work. The epidemiological cutoff values (ECOFFs) or clinical susceptibility breakpoints were retrieved from references 103 and 104.

who underwent lung resection surgery after 5 weeks of clarithromycin treatment at 1,000 mg QD. Simulations adequately predicted the concentration in tissue with the highest accuracy in lung and outer caseum (Fig. 3). The model predictions were somewhat greater than the concentration measured in cellular lesions and somewhat lower than concentrations of inner caseum. This reflects the observation that macrolides slowly diffuse into nonvascularized caseum and that achieving steady state in caseum requires more than the three daily doses required to achieve steady state in rabbit plasma. To select lesion-relevant pharmacodynamic targets, *in vitro* data were used that best represented the expected replication status and microenvironment of the compartment. Specifically, clarithromycin concentrations in lung and cellular lesions, where bacteria are essentially intracellular, were compared to intramacrophage potency values, including concentrations that inhibit 90% growth ($macIC_{90}$) and minimum bactericidal concentration ($macMBC_{90}$). In these cellular and well-perfused compartments, we simulated the concentration-time profiles of total (bound and unbound) drug (Fig. 4, dark gray shaded profile), as well as the free plasma concentrations to reflect passive diffusion of free drug from plasma to interstitial lung tissue (Fig. 4, light gray shaded profile) (68). Even under the assumption that free plasma equilibrates withing interstitial lung and cellular lesion, these free clarithromycin levels were above the $macIC_{90}$ during the entire dosing interval, including in the lower 5th percentile of simulations, indicating high coverage for all patients. Under the scenario of free drug equilibration across compartments, the $macMBC_{90}$ was not achieved in lung and cellular lesions. Using total clarithromycin concentrations in lung and cellular lesion, PD target achievement could not be firmly established due to the limited (less than 10-fold kill, i.e., MBC_{90} not reached) bactericidal activity at the highest concentration tested (Fig. 4). Similar results have been reported by others (69). Clarithromycin concentrations measured by laser capture microdissection in outer and inner caseum, and in bulk cavity caseum, where bacteria are extracellular, were compared to the MIC_{90} and MBC_{90} against biofilms, revealing adequate bacteriostatic coverage throughout the dosing interval, but lack of bactericidal coverage. Because the highest concentration tested against *M. avium* biofilms (20 μg/mL) while inactive is within the range of concentrations achieved in the outer caseous rim, one cannot exclude that potentially bactericidal concentrations might be reached in caseous areas directly adjacent to the cellular rim or in very small necrotic foci (Fig. 4 and Table 4).

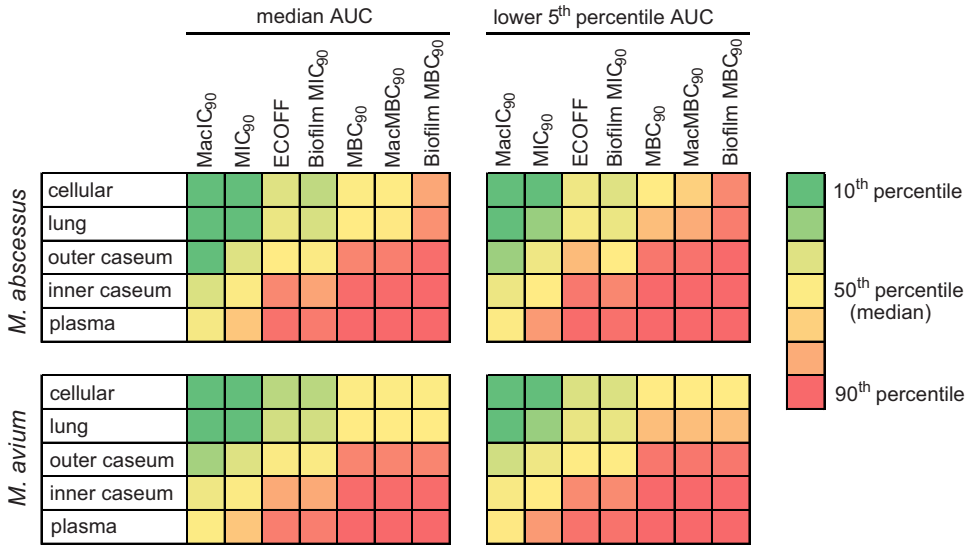

FIG 5 Predicted target attainment expressed as AUC/potency across compartments against *M. abscessus* and *M. avium* disease. The analysis was performed for a range of bacteriostatic and bactericidal potency values and included simulated patients with either average clarithromycin exposure or at the lower end (5th percentile) of the drug exposure spectrum. Color coding spans from dark green (top 10th percentile of ratios or maximum coverage) to dark red (90th percentile or lower 10th percentile of ratios, indicating poor PK-PD coverage).

As a reference, plasma concentrations were compared to the MIC range published as epidemiological cutoff (ECOFF) values, MIC_{90}, and MBC_{90} against replicating bacterial populations in standard media (Table 4). Interestingly, differential PK-PD coverage was observed in subjects with average PK profiles compared to subjects at the lower end (5th percentile) of drug exposure. Median plasma concentrations were above the MIC_{90} against both species during most of the dosing interval, while plasma concentrations of subjects with suboptimal PK achieved the MIC_{90} only during a limited fraction of the dosing interval.

To visualize target attainment across compartments in patients with average exposure or at the lower end of the drug exposure spectrum, we compiled the ratios between AUC and various PD parameters against *M. abscessus* and *M. avium* (Fig. 5 and Fig. S6). Thus, across tissue compartments, clarithromycin was above growth inhibitory concentrations and below bactericidal concentrations against both *M. abscessus* and *M. avium*, and suboptimal PK exposure did not significantly impact target attainment against either pathogen, in line with lesion coverage being primarily driven by PD rather than PK.

DISCUSSION

Among the factors contributing to the poor success rates of the very long NTM-PD treatment with multiple antibiotics is the repurposed nature of all drugs in clinical use, which have not been developed to reach optimal PK-PD targets against NTM pathogens (70). Apart from a phase II trial of inhaled amikacin completed in 2016 (71), very few clinical trials, mostly comparing the efficacy of macrolide-including versus nonmacrolide regimens, against NTM lung infection have been conducted (54, 72, 73). In the case of *M. abscessus* disease, there is no reliable cure (74). In developed countries, the public health situation is significantly more dreadful for NTM-PD than for TB, owing to (i) the intrinsic drug resistance of NTM pathogens (74), (ii) the lack of bactericidal activity of most NTM antibiotics active against NTMs (75), and (iii) the ability of NTM pathogens to acquire a drug-tolerant state in extracellular cords and biofilms (20, 40, 76). In common with TB is the role of the pulmonary pathophysiology in limiting drug penetration to the sites of disease.

Here, we report the distribution and PK-PD of clarithromycin in lung lesions, using a rabbit model of NTM-PD-like pathology and a panel of relevant potency values. This is the first study focusing on the lesion PK-PD of an NTM drug, primarily due to the lack

of an animal model of NTM disease presenting large, organized lesions adequate for drug quantitation in cellular and necrotic compartments. To validate the use of the active TB rabbit model for predicting antibiotic penetration in NTM-PD lesions, we showed that similar lesion types and lesion structure were found in resected lungs from a patient with *M. abscessus* disease, TB patients, and rabbits with chronic active TB. This finding was expected given the considerable overlap in immunopathology and radiographic features of pulmonary TB and NTM-PD (16–18). Compared to murine models, the rabbit model is both time and resource intensive, requiring 12 to 16 weeks of infection to deliver the desired immunopathology, and administration of relatively large amounts of drug or development candidates.

We found that growth-inhibitory clarithromycin concentrations corrected for protein binding were exceeded throughout the dosing interval in cellular lesions and moderately infiltrated lung tissue devoid of grossly visible lesions. In these pulmonary compartments, *M. avium* and *M. abscessus* are thought to reside within immune cells, mostly macrophages and neutrophils (18, 77), as well as epithelial cells. Though clarithromycin showed favorable distribution across lesion compartments, it is expected to only inhibit growth of *M. avium* and *M. abscessus* given its lack of bactericidal activity against replicating and nonreplicating bacterial populations, intracellular bacteria in macrophages, and biofilm persisters found in lung lesions (40). Thus, clarithromycin's clinical activity at the site of infection appears to be PD rather than PK limited, at least against *M. abscessus* and *M. avium*. Other clinically relevant NTM species were not investigated in this study. Notably, free plasma concentrations were below the susceptibility breakpoints of 2 and 4 μg/mL for *M. avium* and *M. abscessus*, respectively, during the entire dosing interval.

The high partitioning of clarithromycin in diseased lung and lesions matched the high uptake in human peripheral blood mononuclear cells-derived macrophages and foamy macrophages *in vitro*, with an enrichment factor of approximately 100-fold. Similarly high uptake has been reported for macrolides monocytes and macrophages (78, 79) and was even higher in polymorphonuclear leukocytes (25, 26, 80), which have been proposed to act as antibiotic Trojan horses (29, 31). In lung resections performed for other indications such as malignancy, favorable but lower (~30-fold) partitioning of clarithromycin was measured in healthy lung tissue relative to plasma (81), consistent with high penetration driven by the much higher abundance of immune cells in NTM- and TB-infected lung than in relatively healthier lung tissue. Collectively, results accumulated by our group with this and other drug classes (82–85) indicate that intracellular-to-extracellular concentration ratios in the macrophage uptake assay are predictive of total cellular lesion-to-plasma concentration ratios *in vivo*. If we assume passive diffusion of unbound drug from plasma into interstitial pulmonary tissue and assume that unbound drug concentrations drive the pharmacological response, unbound clarithromycin remains above the $MacIC_{90}$ in lung and lesions for the entire dosing interval, even in subjects with suboptimal drug exposure.

In cavity caseum and necrotic centers of large granulomas, we observed a decreasing concentration gradient after three daily doses in rabbits, from the outer rim to the inner core of the caseous center, but not in patients who were in advanced steady state. This slow spatial and temporal diffusion of macrolides into nonvascularized caseum is likely driven by their high nonspecific binding to caseum macromolecules (Table 1). In addition, foamy macrophages and other immune cells in which macrolides accumulate may act as a reservoir (26) from which the drugs are slowly released to gradually equilibrate at the caseum-cellular interface and into deep caseum. Based on the similar plasma PK (59), uptake in macrophages and foamy macrophages, and nonspecific binding to caseum macromolecules of azithromycin and clarithromycin, one would expect similar dynamics of partitioning between the cellular and necrotic lesion compartments for both drugs, as suggested by the sparse clinical data obtained here (Fig. 2C). This needs to be confirmed with additional preclinical or clinical samples dosed with azithromycin.

What are the implications of these findings for NTM-PD treatment practice? Our *in vitro* and *in vivo* results consistently show high total concentrations within immune cells and in cellular lesions and minimally involved lung tissue. Although one can expect high nonspecific binding inside immune cells, the pharmacologically active fraction in this microenvironment is

a function of the binding dynamics of the macrolides between their bacterial target and host cell macromolecules. The sustained presence of very high total intracellular concentrations, in excess of 100 μg/mL, upon multimonth therapy may favor bactericidal activity. Recent work measuring the activity of clarithromycin over 7 and 14 days against replicating *M. abscessus* surprisingly revealed bactericidal activity at concentrations of 16 μg/mL and above (39). In addition, the host- and pathogen-targeted anti-inflammatory properties of macrolides are beneficial in controlling harmful inflammatory responses during acute and chronic bacterial infections (86–88). Thus, subjects with minimal necrosis, mostly cellular nodules, consolidations, and miliary disease, may respond better to macrolides. This type of immunopathology is more frequently seen in immunocompromised patients, a growing population due to increasing use of organ transplantation, stem cell transplants, and the widespread use of immunosuppressive therapies for patients with cancer and immune-mediated inflammatory disease (3). In caseum where bacteria are extracellular or within biofilm-like structures, the window between achieved free concentrations and inhibitory concentrations is much narrower than in cellular compartments (Fig. 4), potentially indicative of more limited activity. However, macrolides have been shown to prevent the production of factors involved in the formation of biofilm in both Gram-positive and Gram-negative bacteria (89), including at subinhibitory concentrations. Though this macrolide property has not been reported in NTM, it could contribute, if demonstrated, to the observed biofilm growth inhibitory effect (40, 90) and possibly weaken the dynamic life cycle of established biofilms. Indeed, macrolides are known to alter the structure and architecture of *Pseudomonas* and staphylococcal biofilms via inhibition of polysaccharide synthesis (91, 92). A structurally impaired biofilm may allow for enhanced phagocytosis and clearance of bacteria (93). Considering these results as well as recent findings on the long-term bactericidal activity of clarithromycin against *M. abscessus* cultures (39), further investigations are warranted to better define the role of macrolides in patients with cavitary disease and determine whether patients would benefit from tailored regimens that take the extent of disease pathology and presence of cavity into consideration.

The predicted human-equivalent dose of 200 mg/kg delivered slightly lower than expected exposure owing to the increased clearance in infected rabbits compared to uninfected. Modeling of the infected and uninfected plasma PK concentrations, we found that the 2-compartment model with Michaelis-Menten elimination and Weibull function absorption best fit the data. While the structural model appropriately matched the published model (55), there was uncertainty in estimating the absorption parameter (relative standard error [RSE], 145.9%), possibly due to the inherent variability of clarithromycin absorption in rabbits. Despite the uncertainty, the Weibull function provided an appropriate model fit. Michaelis-Menten elimination is consistent with clarithromycin inhibiting its own metabolism via P-glycoprotein (94). We also acknowledge that human subjects undergo lung resection due to drug recalcitrant disease associated with severe pathology. Thus, the two subjects who contributed resected tissue may not be representative of the typical immunohistology and lesion distribution of mycobacterial lung disease. The small clinical sample size constitutes an additional limitation of the study. A prospective lesion pharmacokinetic study (48) is required to quantify the diffusion kinetics of macrolides into large necrotic foci and cavity caseum.

In summary, we have leveraged the rabbit model of active chronic TB to quantify the penetration of NTM-PD antibiotics at the site of lung infection. The model encompasses the typical immunopathology seen in immunocompromised and immunocompetent patients, namely, cellular nodules, consolidations, necrotic lesions, and cavities (2, 6, 18). By combining standard analytical quantitation with laser-capture microdissection, the methodology delivers spatial quantitation of the drugs of interest in complex lesions. Using macrolides as an initial case study, we have shown that potency limits their efficacy more than penetration to the sites of infection. Our results provide the first step toward the simulation of lesion PK-PD coverage by multidrug combinations. By systematically applying the model and methodology to all approved NTM antibiotics, we hope to identify site-of-disease PK-PD factors contributing to the long duration and poor cure rates of NTM-PD treatment. Similar prospective studies with discovery compounds and clinical development candidates will, in turn, guide the rational

design of better regimens combining agents that together reach and kill all bacterial subpopulations, and the prioritization of most promising regimens for clinical trials, an emerging paradigm in TB drug development (95).

MATERIALS AND METHODS

Clinical research study design and human subjects. One adult with pulmonary MDR-TB scheduled for elective lung resection surgery was asked to participate in the Pharmacokinetics of Standard First and Second Line Anti-TB Drugs in the Lung and Lesions of Subjects Elected for Resection Surgery study (ClinicalTrials.gov ID NCT00816426). The subject had received 1,000 mg daily doses of clarithromycin for 5 weeks (subject 1 in reference 48). The institutional review boards of the National Institute of Allergy and Infection Disease, National Institutes of Health, Bethesda, Maryland, United States, and the Asan Medical Center, Seoul, Republic of Korea, approved the study. All procedures were in accordance with the ethical standards of the Helsinki Declaration. During the surgery, the exact time of pulmonary artery ligation was recorded and used to calculate the time of drug administration relative to surgery, or 31 h.

One adult with chronic *Mycobacterium abscessus* infection scheduled for elective surgery at the NIH Clinical Center gave written consent to participate under NIAID Study of Mycobacterial Infections (ClinicalTrials.gov ID NCT00018044). This participant had pulmonary nontuberculous mycobacterial disease presenting with cavitary lesions, well-organized necrotizing granulomas, and nonnecrotizing granulomas similar to those described previously in lung disease caused by non-TB mycobacteria and *M. tuberculosis*. This 73-year-old female participant received 250 mg azithromycin (AZI), 600 mg rifampin (RIF), 100 mg cefazolin (CFZ), and 900 ethambutol as part of her standard drug regimen for 2 years prior to lung resection. Vessel ligation occurred 26 h after the last AZI dose. Upon lung resection, tissues were either fixed in 4% paraformaldehyde for histopathology staining, weighed, and rapidly frozen at −80°C for homogenization and drug quantitation or snap frozen in liquid nitrogen vapor for sectioning and laser capture microdissection (48).

Pharmacokinetic studies in naive rabbits. Pharmacokinetic studies in uninfected New Zealand White (NZW) rabbits were performed in biosafety level 2 facilities and approved by the Institutional Animal Care and Use Committee of the New Jersey Medical School, Rutgers University, Newark, New Jersey. Groups of four rabbits received a single dose or three daily doses of conjugated linoleic acid (CLA) formulated in 0.5% carboxymethyl cellulose (CMC) and 0.5% Tween 80 by oral gavage. Blood was collected in K_2-EDTA coated tubes from the central ear artery of each rabbit predose and at several time points between drug administration and necropsy (typically 0.5, 1, 2, 4, 6, 8, and 24 h following drug administration). Blood samples were centrifuged at 6,000 rpm for 5 min, and plasma supernatants were transferred and stored at −80°C until they were analyzed by high-pressure liquid chromatography coupled to tandem mass spectrometry (LC-MS/MS).

Rabbit infection, drug administration, and blood collection. All rabbit infection studies were performed in biosafety level 3 facilities and approved by the Institutional Animal Care and Use Committee of the New Jersey Medical School, Rutgers University, Newark, New Jersey, and of the Center for Discovery and Innovation, Hackensack Meridian Health, Nutley, New Jersey. Female NZW rabbits (Charles River Laboratories), weighing 2.2 to 2.6 kg, were maintained under specific-pathogen-free conditions and offered water and chow *ad libitum*. The rabbits were infected with *M. tuberculosis* HN878, using a nose-only aerosol exposure system as described (96). At defined time points from 12 to 16 weeks postinfection (at which point rabbits harbor a spectrum of cellular and necrotic lesions representative of human pathology), rabbits received three daily doses of 200 mg/kg CLA formulated in 0.5% CMC and 0.5% Tween 80 by oral gavage. Blood was collected from the central ear artery of each rabbit predose and at several time points between drug administration and necropsy (typically 0.5, 1, 2, 4, 6, and 24 h or until the time of necropsy). Groups of 3 rabbits were euthanized at 6 and 24 h postdose. These time points were selected based on the plasma PK profile to capture the end of the distribution phase (6 h) and the trough, or C_{min} (24 h). Plasma was prepared as described above and stored at −80°C until analysis by LC-MS/MS.

Lesion dissection and processing. The right and left lungs were removed and weighed for analytical drug measurement and histopathology. From each lung lobe, individual granulomas and uninvolved (nondiseased) lung tissue sections were dissected, sized, weighed, and recorded. Lesions weighing less than 5 mg were pooled. Special care was taken to remove the uninvolved lung tissue surrounding each granuloma. The samples collected from each rabbit were classified as uninvolved lung, necrotic or cellular granulomas, cavity wall, or cavity caseum. When feasible, cavity caseum was separated from the cavity wall to be stored and analyzed separately. Lesions collected for laser-capture microdissection were left embedded in the surrounding tissue and snap frozen in liquid nitrogen vapor as described previously (64). All samples were stored in individual 2-mL tubes at −80°C.

Prior to drug quantitation by LC-MS/MS, all tissue samples were homogenized in 9 volumes of phosphate-buffered saline (PBS). Homogenization of all tissue samples was achieved using a FastPrep-24 instrument (MP Biomedicals) and 1.4-mm zirconium oxide beads (Precellys).

Analytical method for macrolide quantitation. Azithromycin and clarithromycin were purchased from Sigma-Aldrich. Azithromycin-d5 and clarithromycin-d4 internal standards were purchased from Toronto Research Chemicals. Drug-free K_2-EDTA plasma and lungs from NZW rabbits were obtained from BioIVT for use as blank matrices to build standard curves. Neat 1-mg/mL dimethyl sulfoxide (DMSO) stocks for CLA and azithromycin were serial diluted in 50:50 acetonitrile/water to create standard curves and quality control (QC) spiking solutions. Spiked matrix standards and QCs were created by adding 10 μL of spiking solutions to 90 μL of drug-free plasma or control lung homogenate. Extraction was performed for standards, QCs, and study samples by adding 200 μL of 1:1 acetonitrile (ACN)/methanol (MeOH) containing 10 ng/mL stable labeled clarithromycin-d4 and azithromycin-d5 to 20 μL of plasma or homogenized tissue sample and 20 μL of 1:1 ACN/H_2O.

LC-MS/MS analysis was performed on a Sciex Qtrap 6500+ triple-quadrupole mass spectrometer coupled to a Shimadzu Nexera X2 ultra-high-performance liquid chromatography (UHPLC) system to quantify

each drug in plasma. Chromatography was performed on an Agilent Zorbax SB-C_8 column (2.1 by 30 mm; particle size, 3.5 μm) using a reverse-phase gradient elution with aqueous. Milli-Q deionized water with 0.1% formic acid (FA) was used for the aqueous mobile phase and 0.1% FA in ACN for the organic mobile phase. Multiple-reaction monitoring (MRM) of precursor/fragment transitions in electrospray positive ionization mode was used to quantify the analytes. MRM transitions of 749.38/591.30, 754.37/596.30, 748.32/590.30, and 752.33/162.10 were used for azithromycin, azithromycin-d5, clarithromycin, and clarithromycin-d4, respectively. Sample analysis was accepted if the concentrations of the quality control samples were within 20% of the nominal concentration. Data processing was performed using Analyst software (version 1.6.3; Sciex).

Laser-capture microdissection of rabbit and human lesion sections. Twenty-five-micrometer-thick tissue sections were cut from γ-irradiated rabbit lung biopsy specimens using a Leica CM 1860 UV (Buffalo Grove, IL) and thaw mounted onto 1.4-μm-thick Leica polyester (PET) membrane FrameSlides for laser capture microdissection. Tissue sections were immediately stored in sealed containers at −80°C. Adjacent 10-μm-thick tissue sections were thaw mounted onto standard glass microscopy slides for hematoxylin and eosin (H&E) and Ziehl-Neelsen staining. Cellular, necrotic (caseum), and uninvolved lung lesion areas totaling 3 million μm^2 were dissected from between 3 to 5 serial lung biopsy tissue sections using a Leica LMD7 system. The total tissue volume of each pooled sample was determined based on the surface area of the pooled sections and the 25-μm tissue thickness. Areas of cellular and caseous lesion were identified optically from the brightfield image scan and by comparison to the adjacent H&E reference tissue. Pooled dissected lesion tissues were collected into 0.25-mL standard PCR tubes and immediately transferred to −80°C.

Neat 1 mg/mL DMSO stocks for all compounds were diluted serially in 50:50 ACN/H_2O to create standard curves and quality control spiking solutions. We added 2 μL of neat spiking solutions to 2 μL of lesion homogenate prior to extraction. We added 2 μL of ACN/H_2O and 2 μL of PBS to the dissected study samples. Extraction was performed by adding 50 μL of extraction solution ACN/MeOH (1:1) with 5 ng/mL clarithromycin-d4 and azithromycin-d5. Extracts were vortexed for 5 min and centrifuged at 10,000 rpm for 5 min. Forty microliters of supernatant was transferred for LC-MS/MS analysis and diluted with an additional 40 μL of Milli-Q water. LC-MS parameters are described above.

Drug potency assays. Minimum inhibitory and bactericidal concentrations were measured as previously described (97). For growth inhibition and bactericidal assays against intracellular bacteria, we used the protocol of Lefebvre et al. (98) with minor modifications. THP-1 cells were obtained from the American Type Culture Collection (ATCC) and cultured in RPMI 1640 medium supplemented with 10% fetal bovine serum (FBS; Gibco) at 37°C in a humidified CO_2 incubator. THP-1 (10^5 cells per well) were seeded into 96-well plates and differentiated for 24 h by adding 500 ng/mL of phorbol-12-myristate-13-acetate (PMA). The resulting macrophages were washed three times with PBS and infected with *M. abscessus* ATCC 19977 or *M. avium* 11 (99) at a multiplicity of infection (MOI) of 10 for 3 h. The infected macrophages were washed three times with PBS to remove extracellular mycobacteria and treated with clarithromycin as indicated for 3 (*M. abscessus*) or 4 (*M. avium*) days. To enumerate intracellular surviving bacteria, cells were washed three times with PBS and then lysed with PBS and 0.1% Triton X-100. Tenfold serial dilutions were performed using 96-well plates containing 180 μL of PBS, and each dilution was plated onto Middlebrook 7H10 agar. CFU were counted after 4 days of incubation. Macrophage viability was assessed by trypan blue exclusion test. Each experiment included technical duplicates, and the experiments were performed twice independently.

Macrophage uptake and caseum binding assays. Human monocytes were isolated from fresh packed leucocytes (New York Blood Center), purified, activated, and differentiated into foamy macrophages as described in reference 47. Uptake of clarithromycin and azithromycin in primary nonfoamy and foamy macrophages was carried out as described (47), and the incubation concentration was 20 μM for both drugs. Nonspecific drug binding in cavity caseum was measured as described in references 49 and 100.

Modeling of tissue distribution and PK-PD simulations. Data from 100- and 300-mg/kg single doses of CLA in uninfected rabbits were used to develop a plasma PK model. Simulations were performed to match exposure in rabbits predicted to be equivalent to a 200-mg/kg dose in humans. To describe the movement of drug from plasma to the sites of action, a population approach using nonlinear mixed-effects modeling in NONMEM was used. A population plasma PK model was built using data from both infected and uninfected rabbits (Fig. 2). One- and two-compartment distribution compartments were tested. Saturated clearance was tested using Michaelis-Menten kinetics equation (equation 1).

$$\text{Rate of elimination} = -\frac{V_{\max} \times C_{\text{plasma}}}{k_m + C_{\text{plasma}}} \quad (1)$$

First order, zero order, transit compartment, Weibull function (65), flip-flop, and first order with a lag period were tested to fit the absorption phase. Replacing first-order absorption with Weibull absorption function significantly improved model fit (delta objective function value [dOFV], −52.743). Interindividual variability was added to F1, apparent bioavailability (F1) (dOFV, −82.377). The Weibull absorption is defined by equations 2 and 3, where K_w is the absorption rate constant, T_w is time after dose, and lambda (λ) is the shape parameter.

$$\text{WB} = \left(1 - e^{-\text{K}_w \cdot {T_w}^{\lambda}}\right) \quad (2)$$

$$\frac{\text{dA}_{\text{abs}}}{\text{dt}} = -\text{WB} \times A_{\text{abs}} \quad (3)$$

Infection status and weight were tested as covariates. Interindividual variability was tested on bioavailability, volume of distribution, and clearance. To estimate extent of partitioning to the sites of action, the parameters of the final plasma model were fixed, and effect compartments were added for each tissue type as previously

described (33, 83, 101). For the plasma-to-lesion model, the plasma-to-uninvolved lung rate constant was fixed at 10/h given the rapid equilibration half-life of 4 min. Fixing the rate to higher values did not change the other parameter estimates (partition coefficient) significantly. Tissue density was assumed to be 1 g/mL of homogenate. Data obtained with tissue samples processed as homogenates and samples collected by laser-capture microdissection were pooled and treated as equal. Data for the two cavity caseum samples were merged with outer caseum data points based on gross pathology and histology data because no data were available at or near C_{max} for this compartment. A rate ($k_{pl\text{-}lesion}$) ratio or coefficient of penetration ($PC_{pl\text{-}lesion}$), and residual error were estimated for each lesion type. The structural model is shown in equation 4.

$$\frac{dC_{lesion}}{dt} = k_{pl-lesion}(PC_{pl-lesion} \times C_{plasma} - C_{lesion}) \quad (4)$$

Model building was guided by goodness-of-fit plots, objective function value, and visual predictive checks. One thousand simulations, using interindividual variability and residual error as variability, were performed to confirm model fit. NONMEM version 7.4.2, R software version 4.0.5, and the R packages ggplot2 and xpose4 were used for model building, data visualization, and simulations.

A rabbit-to-human translational model was developed by linking lesion parameters estimated in rabbits to a previously published clinical plasma PK model (55). Clinical simulations were integrated with *in vitro* PD targets to derive unbound C_{max}, AUC, and fraction of the dosing interval relative to targets. Fraction unbound was assumed to be 0.3 (102). Model diagnostic plots are shown in Fig. 3.

SUPPLEMENTAL MATERIAL

Supplemental material is available online only.

SUPPLEMENTAL FILE 1, PDF file, 3.8 MB.

SUPPLEMENTAL FILE 2, XLSX file, 0.03 MB.

ACKNOWLEDGMENTS

This work was supported by shared instrumentation grant S10-OD023524 from NIH to V.D., R01-AI132374 from NIH-NIAID to T.D., Grand Challenges in Global Health-11 grant from the Bill and Melinda Gates Foundation (37882) and the Wellcome Trust (077381) to a consortium led by Douglas Young at Imperial College, London, and in part by the intramural NIH research programs of the NIAID (C.E.B.) and NHLBI (K.N.O.).

We thank the animal technical team and the analytical chemistry team of the Center for Discovery and Innovation for technical assistance. We are grateful to Chuck Daley for helpful discussions on the clinical use of clarithromycin against NTM-PD.

REFERENCES

1. Cowman S, van Ingen J, Griffith DE, Loebinger MR. 2019. Non-tuberculous mycobacterial pulmonary disease. Eur Respir J 54:1900250. https://doi.org/10.1183/13993003.00250-2019.
2. O'Connell ML, Birkenkamp KE, Kleiner DE, Folio LR, Holland SM, Olivier KN. 2012. Lung manifestations in an autopsy-based series of pulmonary or disseminated nontuberculous mycobacterial disease. Chest 141:1203–1209. https://doi.org/10.1378/chest.11-0425.
3. Henkle E, Winthrop KL. 2015. Nontuberculous mycobacteria infections in immunosuppressed hosts. Clin Chest Med 36:91–99. https://doi.org/10.1016/j.ccm.2014.11.002.
4. Klein JL, Corbett EL, Slade PM, Miller RF, Coker RJ. 1998. Mycobacterium kansasii and human immunodeficiency virus co-infection in London. J Infect 37:252–259. https://doi.org/10.1016/S0163-4453(98)92014-X.
5. Tomashefski JF, Jr., Stern RC, Demko CA, Doershuk CF. 1996. Nontuberculous mycobacteria in cystic fibrosis. An autopsy study. Am J Respir Crit Care Med 154:523–528. https://doi.org/10.1164/ajrccm.154.2.8756832.
6. Swenson C, Zerbe CS, Fennelly K. 2018. Host variability in NTM disease: implications for research needs. Front Microbiol 9:2901. https://doi.org/10.3389/fmicb.2018.02901.
7. Koh WJ, Hong G, Kim K, Ahn S, Han J. 2012. Pulmonary sequestration infected with nontuberculous mycobacteria: a report of two cases and literature review. Asian Pac J Trop Med 5:917–919. https://doi.org/10.1016/S1995-7645(12)60172-2.
8. Merckx JJ, Soule EH, Karlson AG. 1964. The histopathology of lesions caused by infection with unclassified acid-fast bacteria in man. Report of 25 cases. Am J Clin Pathol 41:244–255. https://doi.org/10.1093/ajcp/41.3.244.
9. Smith MB, Molina CP, Schnadig VJ, Boyars MC, Aronson JF. 2003. Pathologic features of Mycobacterium kansasii infection in patients with acquired immunodeficiency syndrome. Arch Pathol Lab Med 127:554–560. https://doi.org/10.5858/2003-127-0554-PFOMKI.
10. Kim YK, Hahn S, Uh Y, Im DJ, Lim YL, Choi HK, Kim HY. 2014. Comparable characteristics of tuberculous and non-tuberculous mycobacterial cavitary lung diseases. Int J Tuber Lung Dis 18:725–729. https://doi.org/10.5588/ijtld.13.0871.
11. Kim C, Park SH, Oh SY, Kim SS, Jo KW, Shim TS, Kim MY. 2017. Comparison of chest CT findings in nontuberculous mycobacterial diseases vs. Mycobacterium tuberculosis lung disease in HIV-negative patients with cavities. PLoS One 12:e0174240. https://doi.org/10.1371/journal.pone.0174240.
12. Miura K, Nakamura M, Taooka Y, Hotta T, Hamaguchi M, Okimoto T, Tsubata Y, Hamaguchi S, Kuraki T, Isobe T. 2020. Comparison of the chest computed tomography findings between patients with pulmonary tuberculosis and those with Mycobacterium avium complex lung disease. Respir Invest 58:137–143. https://doi.org/10.1016/j.resinv.2019.12.006.
13. Shah HH, Holland RH, Meador RS, Webb WR. 1969. The surgical variations of pulmonary infections caused by different species of Mycobacteria. Ann Thorac Surg 7:145–149. https://doi.org/10.1016/s0003-4975(10)66160-7.
14. Yuan MK, Chang CY, Tsai PH, Lee YM, Huang JW, Chang SC. 2014. Comparative chest computed tomography findings of non-tuberculous mycobacterial lung diseases and pulmonary tuberculosis in patients with acid fast bacilli smear-positive sputum. BMC Pulm Med 14:65. https://doi.org/10.1186/1471-2466-14-65.
15. Oshitani Y, Kitada S, Edahiro R, Tsujino K, Kagawa H, Yoshimura K, Miki K, Miki M, Kida H. 2020. Characteristic chest CT findings for progressive cavities in Mycobacterium avium complex pulmonary disease: a retrospective cohort study. Respir Res 21:10. https://doi.org/10.1186/s12931-020-1273-x.
16. Jeong YJ, Lee KS, Koh WJ, Han J, Kim TS, Kwon OJ. 2004. Nontuberculous mycobacterial pulmonary infection in immunocompetent patients:

comparison of thin-section CT and histopathologic findings. Radiology 231:880–886. https://doi.org/10.1148/radiol.2313030833.
17. Kwon YS, Koh WJ. 2014. Diagnosis of pulmonary tuberculosis and nontuberculous mycobacterial lung disease in Korea. Tuberc Respir Dis (Seoul) 77:1–5. https://doi.org/10.4046/trd.2014.77.1.1.
18. Jain D, Ghosh S, Teixeira L, Mukhopadhyay S. 2017. Pathology of pulmonary tuberculosis and non-tuberculous mycobacterial lung disease: facts, misconceptions, and practical tips for pathologists. Semin Diagn Pathol 34:518–529. https://doi.org/10.1053/j.semdp.2017.06.003.
19. Crow HE, King CT, Smith CE, Corpe RF, Stergus I. 1957. A limited clinical, pathologic, and epidemiologic study of patients with pulmonary lesions associated with atypical acid-fast bacilli in the sputum. Am Rev Tuberc 75:199–222. https://doi.org/10.1164/artpd.1957.75.2.199.
20. Fennelly KP, Ojano-Dirain C, Yang Q, Liu L, Lu L, Progulske-Fox A, Wang GP, Antonelli P, Schultz G. 2016. Biofilm formation by Mycobacterium abscessus in a lung cavity. Am J Respir Crit Care Med 193:692–693. https://doi.org/10.1164/rccm.201508-1586IM.
21. Snijder J. 1965. Histopathology of pulmonary lesions caused by atypical mycobacteria. J Pathol Bacteriol 90:65–73. https://doi.org/10.1002/path.1700900107.
22. Griffith DE, Aksamit T, Brown-Elliott BA, Catanzaro A, Daley C, Gordin F, Holland SM, Horsburgh R, Huitt G, Iademarco MF, Iseman M, Olivier K, Ruoss S, von Reyn CF, Wallace RJ, Jr., Winthrop K, ATS Mycobacterial Diseases Subcommittee, American Thoracic Society, Infectious Disease Society of America. 2007. An official ATS/IDSA statement: diagnosis, treatment, and prevention of nontuberculous mycobacterial diseases. Am J Respir Crit Care Med 175:367–416. https://doi.org/10.1164/rccm.200604-571ST.
23. Griffith DE, Aksamit TR. 2012. Therapy of refractory nontuberculous mycobacterial lung disease. Curr Opin Infect Dis 25:218–227. https://doi.org/10.1097/QCO.0b013e3283511a64.
24. Diel R, Ringshausen F, Richter E, Welker L, Schmitz J, Nienhaus A. 2017. Microbiological and clinical outcomes of treating non-Mycobacterium avium complex nontuberculous mycobacterial pulmonary disease: a systematic review and meta-analysis. Chest 152:120–142. https://doi.org/10.1016/j.chest.2017.04.166.
25. Bosnar M, Kelneric Z, Munic V, Erakovic V, Parnham MJ. 2005. Cellular uptake and efflux of azithromycin, erythromycin, clarithromycin, telithromycin, and cethromycin. Antimicrob Agents Chemother 49:2372–2377. https://doi.org/10.1128/AAC.49.6.2372-2377.2005.
26. Wildfeuer A, Laufen H, Zimmermann T. 1996. Uptake of azithromycin by various cells and its intracellular activity under in vivo conditions. Antimicrob Agents Chemother 40:75–79. https://doi.org/10.1128/AAC.40.1.75.
27. Labro MT. 1996. Intracellular bioactivity of macrolides. Clin Microbiol Infect 1(Suppl 1):S24–S30. https://doi.org/10.1111/j.1469-0691.1996.tb00588.x.
28. Gladue RP, Bright GM, Isaacson RE, Newborg MF. 1989. In vitro and in vivo uptake of azithromycin (CP-62,993) by phagocytic cells: possible mechanism of delivery and release at sites of infection. Antimicrob Agents Chemother 33:277–282. https://doi.org/10.1128/AAC.33.3.277.
29. Frank MO, Sullivan GW, Carper HT, Mandell GL. 1992. In vitro demonstration of transport and delivery of antibiotics by polymorphonuclear leukocytes. Antimicrob Agents Chemother 36:2584–2588. https://doi.org/10.1128/AAC.36.12.2584.
30. Nakamura S, Yanagihara K, Araki N, Yamada K, Morinaga Y, Izumikawa K, Seki M, Kakeya H, Yamamoto Y, Kamihira S, Kohno S. 2010. Efficacy of clarithromycin against experimentally induced pneumonia caused by clarithromycin-resistant Haemophilus influenzae in mice. Antimicrob Agents Chemother 54:757–762. https://doi.org/10.1128/AAC.00524-09.
31. Amsden GW. 2001. Advanced-generation macrolides: tissue-directed antibiotics. Int J Antimicrob Agents 18(Suppl 1):S11–5. https://doi.org/10.1016/S0924-8579(01)00410-1.
32. Alffenaar JW, Martson AG, Heysell SK, Cho JG, Patanwala A, Burch G, Kim HY, Sturkenboom MGG, Byrne A, Marriott D, Sandaradura I, Tiberi S, Sintchencko V, Srivastava S, Peloquin CA. 2021. Therapeutic drug monitoring in non-tuberculosis mycobacteria infections. Clin Pharmacokinet 60:711–725. https://doi.org/10.1007/s40262-021-01000-6.
33. Strydom N, Gupta SV, Fox WS, Via LE, Bang H, Lee M, Eum S, Shim T, Barry CE, III, Zimmerman M, Dartois V, Savic RM. 2019. Tuberculosis drugs' distribution and emergence of resistance in patient's lung lesions: a mechanistic model and tool for regimen and dose optimization. PLoS Med 16:e1002773. https://doi.org/10.1371/journal.pmed.1002773.
34. Brown-Elliott BA, Nash KA, Wallace RJ, Jr. 2012. Antimicrobial susceptibility testing, drug resistance mechanisms, and therapy of infections with nontuberculous mycobacteria. Clin Microbiol Rev 25:545–582. https://doi.org/10.1128/CMR.05030-11.
35. Choi GE, Shin SJ, Won CJ, Min KN, Oh T, Hahn MY, Lee K, Lee SH, Daley CL, Kim S, Jeong BH, Jeon K, Koh WJ. 2012. Macrolide treatment for Mycobacterium abscessus and Mycobacterium massiliense infection and inducible resistance. Am J Respir Crit Care Med 186:917–925. https://doi.org/10.1164/rccm.201111-2005OC.
36. Richard M, Gutierrez AV, Kremer L. 2020. Dissecting erm(41)-mediated macrolide-inducible resistance in Mycobacterium abscessus. Antimicrob Agents Chemother 64:e01879-19. https://doi.org/10.1128/AAC.01879-19.
37. Yoshida S, Tsuyuguchi K, Kobayashi T, Inoue Y, Suzuki K. 2021. Comparison of drug-susceptibility patterns and gene sequences associated with clarithromycin and azithromycin resistance in Mycobacterium abscessus complex isolates and evaluation of the accumulation of intrinsic macrolide resistance. J Med Microbiol 70. https://doi.org/10.1099/jmm.0.001326.
38. Greendyke R, Byrd TF. 2008. Differential antibiotic susceptibility of Mycobacterium abscessus variants in biofilms and macrophages compared to that of planktonic bacteria. Antimicrob Agents Chemother 52:2019–2026. https://doi.org/10.1128/AAC.00986-07.
39. Lee J, Ammerman N, Agarwal A, Naji M, Li SY, Nuermberger E. 2021. Differential in vitro activities of individual drugs and bedaquiline-rifabutin combinations against actively multiplying and nutrient-starved mycobacterium abscessus. Antimicrob Agents Chemother 65:e02179-20. https://doi.org/10.1128/AAC.02179-20.
40. Yam Y-K, Alvarez N, Go M-L, Dick T. 2020. Extreme Drug Tolerance of Mycobacterium abscessus "Persisters". Front Microbiol 11:359. https://doi.org/10.3389/fmicb.2020.00359.
41. Obregon-Henao A, Arnett KA, Henao-Tamayo M, Massoudi L, Creissen E, Andries K, Lenaerts AJ, Ordway DJ. 2015. Susceptibility of Mycobacterium abscessus to antimycobacterial drugs in preclinical models. Antimicrob Agents Chemother 59:6904–6912. https://doi.org/10.1128/AAC.00459-15.
42. Ordway D, Henao-Tamayo M, Smith E, Shanley C, Harton M, Troudt J, Bai X, Basaraba RJ, Orme IM, Chan ED. 2008. Animal model of Mycobacterium abscessus lung infection. J Leukoc Biol 83:1502–1511. https://doi.org/10.1189/jlb.1007696.
43. Riva C, Tortoli E, Cugnata F, Sanvito F, Esposito A, Rossi M, Colarieti A, Canu T, Cigana C, Bragonzi A, Lore NI, Miotto P, Cirillo DM. 2020. A new model of chronic Mycobacterium abscessus lung infection in immunocompetent mice. Int J Mol Sci 21:6590. https://doi.org/10.3390/ijms21186590.
44. Maggioncalda EC, Story-Roller E, Mylius J, Illei P, Basaraba RJ, Lamichhane G. 2020. A mouse model of pulmonary Mycobacteroides abscessus infection. Sci Rep 10:3690. https://doi.org/10.1038/s41598-020-60452-1.
45. Chen RY, Yu X, Smith B, Liu X, Gao J, Diacon AH, Dawson R, Tameris M, Zhu H, Qu Y, Zhang R, Pan S, Jin X, Goldfeder LC, Cai Y, Arora K, Wang J, Vincent J, Malherbe ST, Thienemann F, Wilkinson RJ, Walzl G, Barry CEI. 2021. Radiological and functional evidence of the bronchial spread of tuberculosis: an observational analysis. Lancet Microbe 2:e518–e526. https://doi.org/10.1016/S2666-5247(21)00058-6.
46. Wells G, Glasgow JN, Nargan K, Lumamba K, Madansein R, Maharaj K, Hunter RL, Naidoo T, Coetzer L, Le Roux S, Du Plessis A, Steyn AJC. 2021. Micro–computed tomography analysis of the human tuberculous lung reveals remarkable heterogeneity in three-dimensional granuloma morphology. Am J Respir Crit Care Med 204:583–595. https://doi.org/10.1164/rccm.202101-0032OC.
47. Blanc L, Daudelin IB, Podell BK, Chen PY, Zimmerman M, Martinot AJ, Savic RM, Prideaux B, Dartois V. 2018. High-resolution mapping of fluoroquinolones in TB rabbit lesions reveals specific distribution in immune cell types. Elife 7:e41115. https://doi.org/10.7554/eLife.41115.
48. Prideaux B, Via LE, Zimmerman MD, Eum S, Sarathy J, O'Brien P, Chen C, Kaya F, Weiner DM, Chen PY, Song T, Lee M, Shim TS, Cho JS, Kim W, Cho SN, Olivier KN, Barry CE, III, Dartois V. 2015. The association between sterilizing activity and drug distribution into tuberculosis lesions. Nat Med 21:1223–1227. https://doi.org/10.1038/nm.3937.
49. Sarathy JP, Zuccotto F, Hsinpin H, Sandberg L, Via LE, Marriner GA, Masquelin T, Wyatt P, Ray P, Dartois V. 2016. Prediction of drug penetration in tuberculosis lesions. ACS Infect Dis 2:552–563. https://doi.org/10.1021/acsinfecdis.6b00051.
50. Je S, Quan H, Na Y, Cho SN, Kim BJ, Seok SH. 2016. An in vitro model of granuloma-like cell aggregates substantiates early host immune responses against Mycobacterium massiliense infection. Biol Open 5:1118–1127. https://doi.org/10.1242/bio.019315.
51. Peyron P, Vaubourgeix J, Poquet Y, Levillain F, Botanch C, Bardou F, Daffe M, Emile JF, Marchou B, Cardona PJ, de Chastellier C, Altare F. 2008. Foamy macrophages from tuberculous patients' granulomas constitute a nutrient-rich reservoir for M. tuberculosis persistence. PLoS Pathog 4:e1000204. https://doi.org/10.1371/journal.ppat.1000204.

52. Prosser G, Brandenburg J, Reiling N, Barry CE, III, Wilkinson RJ, Wilkinson KA. 2017. The bacillary and macrophage response to hypoxia in tuberculosis and the consequences for T cell antigen recognition. Microbes Infect 19:177–192. https://doi.org/10.1016/j.micinf.2016.10.001.
53. Ryu YJ, Koh WJ, Daley CL. 2016. Diagnosis and treatment of nontuberculous mycobacterial lung disease: clinicians' perspectives. Tuberc Respir Dis (Seoul) 79:74–84. https://doi.org/10.4046/trd.2016.79.2.74.
54. Daley CL, Iaccarino JM, Lange C, Cambau E, Wallace RJ, Andrejak C, Bottger EC, Brozek J, Griffith DE, Guglielmetti L, Huitt GA, Knight SL, Leitman P, Marras TK, Olivier KN, Santin M, Stout JE, Tortoli E, van Ingen J, Wagner D, Winthrop KL. 2020. Treatment of nontuberculous mycobacterial pulmonary disease: an official ATS/ERS/ESCMID/IDSA clinical practice guideline. Clin Infect Dis 71:905–913. https://doi.org/10.1093/cid/ciaa1125.
55. Abduljalil K, Kinzig M, Bulitta J, Horkovics-Kovats S, Sorgel F, Rodamer M, Fuhr U. 2009. Modeling the autoinhibition of clarithromycin metabolism during repeated oral administration. Antimicrob Agents Chemother 53:2892–2901. https://doi.org/10.1128/AAC.01193-08.
56. Chu S, Wilson DS, Deaton RL, Mackenthun AV, Eason CN, Cavanaugh JH. 1993. Single- and multiple-dose pharmacokinetics of clarithromycin, a new macrolide antimicrobial. J Clin Pharmacol 33:719–726. https://doi.org/10.1002/j.1552-4604.1993.tb05613.x.
57. Chu SY, Sennello LT, Bunnell ST, Varga LL, Wilson DS, Sonders RC. 1992. Pharmacokinetics of clarithromycin, a new macrolide, after single ascending oral doses. Antimicrob Agents Chemother 36:2447–2453. https://doi.org/10.1128/AAC.36.11.2447.
58. Chu SY, Wilson DS, Guay DR, Craft C. 1992. Clarithromycin pharmacokinetics in healthy young and elderly volunteers. J Clin Pharmacol 32:1045–1049. https://doi.org/10.1002/j.1552-4604.1992.tb03809.x.
59. Lebel M. 1993. Pharmacokinetic properties of clarithromycin: a comparison with erythromycin and azithromycin. Can J Infect Dis 4:148–152. https://doi.org/10.1155/1993/168061.
60. Rodvold KA. 1999. Clinical pharmacokinetics of clarithromycin. Clin Pharmacokinet 37:385–398. https://doi.org/10.2165/00003088-199937050-00003.
61. Van Bambeke F, Tulkens PM. 2001. Macrolides: pharmacokinetics and pharmacodynamics. Int J Antimicrob Agents 18:17–23. https://doi.org/10.1016/S0924-8579(01)00406-X.
62. Eyler RF, Shvets K. 2019. Clinical pharmacology of antibiotics. Clin J Am Soc Nephrol 14:1080–1090. https://doi.org/10.2215/CJN.08140718.
63. Jacobs MR. 2001. Optimisation of antimicrobial therapy using pharmacokinetic and pharmacodynamic parameters. Clin Microbiol Infect 7:589–596. https://doi.org/10.1046/j.1198-743x.2001.00295.x.
64. Zimmerman M, Blanc L, Chen PY, Dartois V, Prideaux B. 2018. Spatial quantification of drugs in pulmonary tuberculosis lesions by laser capture microdissection liquid chromatography mass spectrometry (LCM-LC/MS). J Vis Exp 134:e57402. https://doi.org/10.3791/57402.
65. Zhou H. 2003. Pharmacokinetic strategies in deciphering atypical drug absorption profiles. J Clin Pharmacol 43:211–227. https://doi.org/10.1177/0091270002250613.
66. Aziz DB, Low JL, Wu ML, Gengenbacher M, Teo JW, Dartois V, Dick T. 2017. Rifabutin is active against Mycobacterium abscessus complex. Antimicrob Agents Chemother 61:e00155-17. https://doi.org/10.1128/AAC.00155-17.
67. Rodriguez G, Ortegon M, Camargo D, Orozco LC. 1997. Iatrogenic Mycobacterium abscessus infection: histopathology of 71 patients. Br J Dermatol 137:214–218. https://doi.org/10.1046/j.1365-2133.1997.18081891.x.
68. Smith DA, Rowland M. 2019. Intracellular and intraorgan concentrations of small molecule drugs: theory, uncertainties in infectious diseases and oncology, and promise. Drug Metab Dispos 47:665–672. https://doi.org/10.1124/dmd.118.085951.
69. Molina-Torres CA, Tamez-Pena L, Castro-Garza J, Ocampo-Candiani J, Vera-Cabrera L. 2018. Evaluation of the intracellular activity of drugs against Mycobacterium abscessus using a THP-1 macrophage model. J Microbiol Methods 148:29–32. https://doi.org/10.1016/j.mimet.2018.03.020.
70. Kim HY, Sintchenko V, Alffenaar JW. 2019. Nontuberculosis mycobacteria infections: would there be pharmacodynamics without pharmacokinetics? Eur Respir J 54:1901508. https://doi.org/10.1183/13993003.01508-2019.
71. Olivier KN, Griffith DE, Eagle G, McGinnis JP, II, Micioni L, Liu K, Daley CL, Winthrop KL, Ruoss S, Addrizzo-Harris DJ, Flume PA, Dorgan D, Salathe M, Brown-Elliott BA, Gupta R, Wallace RJ, Jr. 2017. Randomized trial of liposomal amikacin for inhalation in nontuberculous mycobacterial lung disease. Am J Respir Crit Care Med 195:814–823. https://doi.org/10.1164/rccm.201604-0700OC.
72. Griffith DE, Daley CL. 2022. Treatment of Mycobacterium abscessus pulmonary disease. Chest 161:64–75. https://doi.org/10.1016/j.chest.2021.07.035.
73. Waters V, Ratjen F. 2012. Antibiotic treatment for nontuberculous mycobacteria lung infection in people with cystic fibrosis. Cochrane Database Syst Rev 12:CD010004. https://doi.org/10.1002/14651858.CD010004.pub2.
74. Johansen MD, Herrmann JL, Kremer L. 2020. Non-tuberculous mycobacteria and the rise of Mycobacterium abscessus. Nat Rev Microbiol 18:392–407. https://doi.org/10.1038/s41579-020-0331-1.
75. Wu M-L, Aziz DB, Dartois V, Dick T. 2018. NTM drug discovery: status, gaps and way forward. Drug Discov Today 23:1502–1519. https://doi.org/10.1016/j.drudis.2018.04.001.
76. Bernut A, Herrmann JL, Kissa K, Dubremetz JF, Gaillard JL, Lutfalla G, Kremer L. 2014. Mycobacterium abscessus cording prevents phagocytosis and promotes abscess formation. Proc Natl Acad Sci U S A 111:E943–52. https://doi.org/10.1073/pnas.1321390111.
77. Malcolm KC, Caceres SM, Pohl K, Poch KR, Bernut A, Kremer L, Bratton DL, Herrmann JL, Nick JA. 2018. Neutrophil killing of Mycobacterium abscessus by intra- and extracellular mechanisms. PLoS One 13:e0196120. https://doi.org/10.1371/journal.pone.0196120.
78. Olsen KM, San Pedro G, Gann LP, Gubbins PO, Halinski DM, Campbell GD, Jr. 1996. Intrapulmonary pharmacokinetics of azithromycin in healthy volunteers given five oral doses. Antimicrob Agents Chemother 40:2582–2585. https://doi.org/10.1128/AAC.40.11.2582.
79. Iskandar I, Walters JD. 2011. Clarithromycin accumulation by phagocytes and its effect on killing of Aggregatibacter actinomycetemcomitans. J Periodontol 82:497–504. https://doi.org/10.1902/jop.2010.100221.
80. Liu P, Allaudeen H, Chandra R, Phillips K, Jungnik A, Breen JD, Sharma A. 2007. Comparative pharmacokinetics of azithromycin in serum and white blood cells of healthy subjects receiving a single-dose extended-release regimen versus a 3-day immediate-release regimen. Antimicrob Agents Chemother 51:103–109. https://doi.org/10.1128/AAC.00852-06.
81. Fish DN, Gotfried MH, Danziger LH, Rodvold KA. 1994. Penetration of clarithromycin into lung tissues from patients undergoing lung resection. Antimicrob Agents Chemother 38:876–878. https://doi.org/10.1128/AAC.38.4.876.
82. Egbelowo O, Sarathy JP, Gausi K, Zimmerman MD, Wang H, Wijnant GJ, Kaya F, Gengenbacher M, Van N, Degefu Y, Nacy C, Aldridge BB, Carter CL, Denti P, Dartois V. 2021. Pharmacokinetics and target attainment of SQ109 in plasma and human-like tuberculosis lesions in rabbits. Antimicrob Agents Chemother 65:e0002421. https://doi.org/10.1128/AAC.00024-21.
83. Ernest JP, Sarathy J, Wang N, Kaya F, Zimmerman MD, Strydom N, Wang H, Xie M, Gengenbacher M, Via LE, Barry CE, III, Carter CL, Savic RM, Dartois V. 2021. Lesion penetration and activity limit the utility of second-line injectable agents in pulmonary tuberculosis. Antimicrob Agents Chemother 65:e00506-21. https://doi.org/10.1128/AAC.00506-21.
84. Sarathy J, Blanc L, Alvarez-Cabrera N, O'Brien P, Dias-Freedman I, Mina M, Zimmerman M, Kaya F, Ho Liang H-P, Prideaux B, Dietzold J, Salgame P, Savic RM, Linderman J, Kirschner D, Pienaar E, Dartois V. 2019. Fluoroquinolone efficacy against tuberculosis is driven by penetration into lesions and activity against resident bacterial populations. Antimicrob Agents Chemother 63:e02516-18. https://doi.org/10.1128/AAC.02516-18.
85. Gengenbacher M, Zimmerman MD, Sarathy JP, Kaya F, Wang H, Mina M, Carter C, Hossen MA, Su H, Trujillo C, Ehrt S, Schnappinger D, Dartois V. 2020. Tissue distribution of doxycycline in animal models of tuberculosis. Antimicrob Agents Chemother 64:e02479-19. https://doi.org/10.1128/AAC.02479-19.
86. Steel HC, Theron AJ, Cockeran R, Anderson R, Feldman C. 2012. Pathogen- and host-directed anti-inflammatory activities of macrolide antibiotics. Mediators Inflamm 2012:584262. https://doi.org/10.1155/2012/584262.
87. Altenburg J, de Graaff CS, van der Werf TS, Boersma WG. 2011. Immunomodulatory effects of macrolide antibiotics - part 1: biological mechanisms. Respiration 81:67–74. https://doi.org/10.1159/000320319.
88. Amsden GW. 2005. Anti-inflammatory effects of macrolides–an underappreciated benefit in the treatment of community-acquired respiratory tract infections and chronic inflammatory pulmonary conditions? J Antimicrob Chemother 55:10–21. https://doi.org/10.1093/jac/dkh519.
89. Parra-Ruiz J, Vidaillac C, Rybak MJ. 2012. Macrolides and staphylococcal biofilms. Rev Esp Quimioter 25:10–16.
90. Carter G, Young LS, Bermudez LE. 2004. A subinhibitory concentration of clarithromycin inhibits Mycobacterium avium biofilm formation. Antimicrob Agents Chemother 48:4907–4910. https://doi.org/10.1128/AAC.48.12.4907-4910.2004.
91. Yasuda H, Ajiki Y, Koga T, Kawada H, Yokota T. 1993. Interaction between biofilms formed by Pseudomonas aeruginosa and clarithromycin. Antimicrob Agents Chemother 37:1749–1755. https://doi.org/10.1128/AAC.37.9.1749.
92. Yasuda H, Ajiki Y, Koga T, Yokota T. 1994. Interaction between clarithromycin and biofilms formed by Staphylococcus epidermidis. Antimicrob Agents Chemother 38:138–141. https://doi.org/10.1128/AAC.38.1.138.

93. Takeoka K, Ichimiya T, Yamasaki T, Nasu M. 1998. The in vitro effect of macrolides on the interaction of human polymorphonuclear leukocytes with Pseudomonas aeruginosa in biofilm. Chemotherapy 44:190–197. https://doi.org/10.1159/000007114.
94. Hughes J, Crowe A. 2010. Inhibition of P-glycoprotein-mediated efflux of digoxin and its metabolites by macrolide antibiotics. J Pharmacol Sci 113:315–324. https://doi.org/10.1254/jphs.10109fp.
95. Ernest J, Strydrom N, Wang Q, Zhang N, Nuermberger E, Dartois VRS. 2020. Development of new tuberculosis drugs: translation to regimen composition for drug-sensitive and multidrug-resistant tuberculosis. Annu Rev of Pharmacol Toxicol 61:495–516. https://doi.org/10.1146/annurev-pharmtox-030920-011143.
96. Tsenova L, Harbacheuski R, Ellison E, Manca C, Kaplan G. 2006. Aerosol exposure system for rabbits: application to M. tuberculosis infection. Appl Biosaf 11:7–14. https://doi.org/10.1177/153567600601100103.
97. Low JL, Wu ML, Aziz DB, Laleu B, Dick T. 2017. Screening of TB actives for activity against nontuberculous mycobacteria delivers high hit rates. Front Microbiol 8:1539. https://doi.org/10.3389/fmicb.2017.01539.
98. Lefebvre AL, Dubee V, Cortes M, Dorchene D, Arthur M, Mainardi JL. 2016. Bactericidal and intracellular activity of beta-lactams against Mycobacterium abscessus. J Antimicrob Chemother 71:1556–1563. https://doi.org/10.1093/jac/dkw022.
99. Yee M, Klinzing D, Wei JR, Gengenbacher M, Rubin EJ, Chien JY, Hsueh PR, Dick T. 2017. Draft genome sequence of Mycobacterium avium 11. Genome Announc 5:e00766-17. https://doi.org/10.1128/genomeA.00766-17.
100. Sarathy JP, Liang HH, Weiner D, Gonzales J, Via LE, Dartois V. 2017. An in vitro caseum binding assay that predicts drug penetration in tuberculosis lesions. J Vis Exp e55559. https://doi.org/10.3791/55559.
101. Rifat D, Prideaux B, Savic RM, Urbanowski ME, Parsons TL, Luna B, Marzinke MA, Ordonez AA, Demarco VP, Jain KK, Dartois V, Bishai WR, Dooley KE. 2018. Using the rabbit cavitary disease model, site-of-disease PK to understand rifamycin trial results for tuberculosis. Sci Transl Med, 10(435):eaai7786. https://doi.org/10.1126/scitranslmed.aai7786.
102. Davey PG. 1991. The pharmacokinetics of clarithromycin and its 14-OH metabolite. J Hosp Infect 19:29–37. https://doi.org/10.1016/0195-6701(91)90215-T.
103. Brown-Elliott BA, Vasireddy S, Vasireddy R, Iakhiaeva E, Howard ST, Nash K, Parodi N, Strong A, Gee M, Smith T, Wallace RJ, Jr. 2015. Utility of sequencing the erm(41) gene in isolates of Mycobacterium abscessus subsp. abscessus with low and intermediate clarithromycin MICs. J Clin Microbiol 53:1211–1215. https://doi.org/10.1128/JCM.02950-14.
104. Schon T, Chryssanthou E. 2017. Minimum inhibitory concentration distributions for Mycobacterium avium complex-towards evidence-based susceptibility breakpoints. Int J Infect Dis 55:122–124. https://doi.org/10.1016/j.ijid.2016.12.027.
105. Tomioka H, Sato K, Sano C, Sano K, Shimizu T. 2002. Intramacrophage passage of Mycobacterium tuberculosis and M. avium complex alters the drug susceptibilities of the organisms as determined by intracellular susceptibility testing using macrophages and type II alveolar epithelial cells. Antimicrob Agents Chemother 46:519–521. https://doi.org/10.1128/AAC.46.2.519-521.2002.
106. McNabe M, Tennant R, Danelishvili L, Young L, Bermudez LE. 2011. Mycobacterium avium ssp. hominissuis biofilm is composed of distinct phenotypes and influenced by the presence of antimicrobials. Clin Microbiol Infect 17:697–703. https://doi.org/10.1111/j.1469-0691.2010.03307.x.
107. Rose SJ, Babrak LM, Bermudez LE. 2015. Mycobacterium avium possesses extracellular DNA that contributes to biofilm formation, structural integrity, and tolerance to antibiotics. PLoS One 10:e0128772. https://doi.org/10.1371/journal.pone.0128772.